

Structural basis of ligand binding modes at the neuropeptide Y Y₁ receptor

Zhenlin Yang^{1,2,15}, Shuo Han^{1,3,15}, Max Keller^{4,15*}, Anette Kaiser^{5,15}, Brian J. Bender^{6,15}, Mathias Bosse⁷, Kerstin Burkert⁵, Lisa M. Kögler⁵, David Wifling⁴, Guenther Bernhardt⁴, Nicole Plank⁴, Timo Littmann⁴, Peter Schmidt⁷, Cuiying Yi¹, Beibei Li^{1,8}, Sheng Ye³, Rongguang Zhang^{3,9}, Bo Xu¹⁰, Dan Larhammar¹⁰, Raymond C. Stevens^{11,12}, Daniel Huster⁷, Jens Meiler^{6,13}, Qiang Zhao^{1,2,8,14}, Annette G. Beck-Sickinger^{5*}, Armin Buschauer^{4,16} & Beili Wu^{1,8,12,14*}

Neuropeptide Y (NPY) receptors belong to the G-protein-coupled receptor superfamily and have important roles in food intake, anxiety and cancer biology^{1,2}. The NPY–Y receptor system has emerged as one of the most complex networks with three peptide ligands (NPY, peptide YY and pancreatic polypeptide) binding to four receptors in most mammals, namely the Y₁, Y₂, Y₄ and Y₅ receptors, with different affinity and selectivity³. NPY is the most powerful stimulant of food intake and this effect is primarily mediated by the Y₁ receptor (Y₁R)⁴. A number of peptides and small-molecule compounds have been characterized as Y₁R antagonists and have shown clinical potential in the treatment of obesity⁴, tumour¹ and bone loss⁵. However, their clinical usage has been hampered by low potency and selectivity, poor brain penetration ability or lack of oral bioavailability⁶. Here we report crystal structures of the human Y₁R bound to the two selective antagonists UR-MK299 and BMS-193885 at 2.7 and 3.0 Å resolution, respectively. The structures combined with mutagenesis studies reveal the binding modes of Y₁R to several structurally diverse antagonists and the determinants of ligand selectivity. The Y₁R structure and molecular docking of the endogenous agonist NPY, together with nuclear magnetic resonance, photo-crosslinking and functional studies, provide insights into the binding behaviour of the agonist and for the first time, to our knowledge, determine the interaction of its N terminus with the receptor. These insights into Y₁R can enable structure-based drug discovery that targets NPY receptors.

NPY is a highly abundant neuropeptide in the central nervous system⁷. The first characterized NPY receptor Y₁R is widely expressed in a variety of tissues and is involved in the regulation of many physiological functions, some of which are known to be related to obesity⁸ and cancer⁹. To better understand the ligand-binding behaviour of NPY receptors and provide a basis for drug discovery, we solved crystal structures of Y₁R in complex with two structurally diverse antagonists, UR-MK299, an argininamide with high Y₁R selectivity¹⁰, and BMS-193885, which displays anorectic activity in animal models⁶ (Fig. 1 and Extended Data Table 1). To facilitate the determination of structure, an engineered Y₁R construct was designed (see ‘Cloning and protein expression’ in Methods).

Within the β-branch of class A G-protein-coupled receptors (GPCRs), to which NPY receptors belong, the structures of four receptors, namely the neurotensin receptor NTS1¹¹, the OX₁ and OX₂ orexin receptors^{12,13} and the endothelin ET_B receptor¹⁴, have been

determined so far. These structures reveal differences of ligand-binding modes between different receptors, suggesting that more structural information is needed to develop any consensus about the ligand recognition mechanisms for this GPCR subfamily. The Y₁R structure shares a canonical seven-transmembrane helical bundle (helices I–VII) with the other known GPCR structures (Fig. 1 and Extended Data Fig. 1a, b). The Y₁R–UR-MK299 and Y₁R–BMS-193885 complexes are structurally similar with a C_α root-mean-square deviation (r.m.s.d.) of 0.75 Å within the helical bundle. Both structures exhibit inactive conformations with helix VI adopting an inward conformation that is similar to other inactive GPCR structures. UR-MK299 binds to Y₁R in a cavity within the helical bundle bordered by helices III, IV, V, VI and VII (Fig. 2a, b). The diphenylmethyl moiety of the antagonist interacts with a hydrophobic cluster formed by F282^{6.54}, F286^{6.58} and F302^{7.35} (superscripts on residues throughout the text indicate Ballesteros–Weinstein nomenclature¹⁵) on helices VI and VII of Y₁R. The critical role of this hydrophobic patch in recognizing the argininamide-type

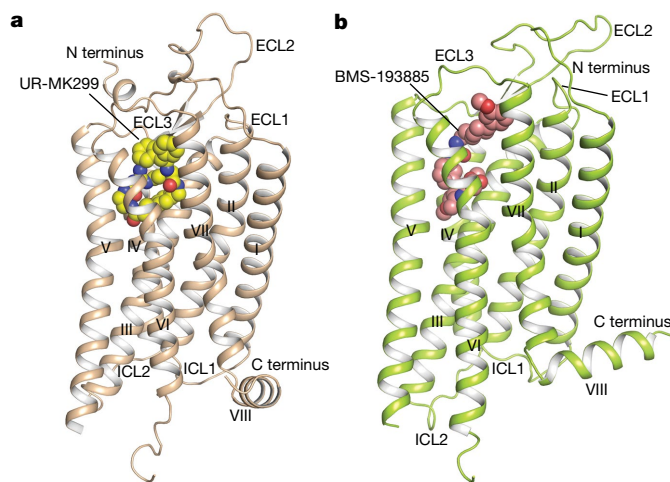


Fig. 1 | Structures of the Y₁R–UR-MK299 and Y₁R–BMS-193885 complexes. **a**, Structure of the Y₁R–UR-MK299 complex. The receptor is shown in brown cartoon representation. UR-MK299 is shown as spheres with carbons in yellow. **b**, Structure of the Y₁R–BMS-193885 complex. The receptor is shown in green cartoon representation. BMS-193885 is shown as spheres with carbons in pink.

¹Chinese Academy of Sciences Key Laboratory of Receptor Research, Shanghai Institute of Materia Medica, Chinese Academy of Sciences, Shanghai, China. ²State Key Laboratory of Drug Research, Shanghai Institute of Materia Medica, Chinese Academy of Sciences, Shanghai, China. ³National Laboratory of Biomacromolecules, Institute of Biophysics, Chinese Academy of Sciences, Beijing, China. ⁴Pharmaceutical/Medicinal Chemistry II, Institute of Pharmacy, University of Regensburg, Regensburg, Germany. ⁵Institute of Biochemistry, Faculty of Life Sciences, Leipzig University, Leipzig, Germany. ⁶Department of Pharmacology, Center for Structural Biology, Vanderbilt University, Nashville, TN, USA. ⁷Institute for Medical Physics and Biophysics, Leipzig University, Leipzig, Germany. ⁸University of Chinese Academy of Sciences, Beijing, China. ⁹National Center for Protein Science Shanghai, Institute of Biochemistry and Cell Biology, Shanghai Institutes for Biological Sciences, Chinese Academy of Sciences, Shanghai, China. ¹⁰Department of Neuroscience, Science for Life Laboratory, Uppsala University, Uppsala, Sweden. ¹¹Human Institute, ShanghaiTech University, Shanghai, China. ¹²School of Life Science and Technology, ShanghaiTech University, Shanghai, China. ¹³Departments of Chemistry and Bioinformatics, Center for Structural Biology, Vanderbilt University, Nashville, TN, USA. ¹⁴Chinese Academy of Sciences Center for Excellence in Biomacromolecules, Chinese Academy of Sciences, Beijing, China. ¹⁵These authors contributed equally: Zhenlin Yang, Shuo Han, Max Keller, Anette Kaiser, Brian J. Bender. ¹⁶Deceased: Armin Buschauer. *e-mail: abeck-sickinger@uni-leipzig.de; max.keller@chemie.uni-regensburg.de; beiliwu@simm.ac.cn

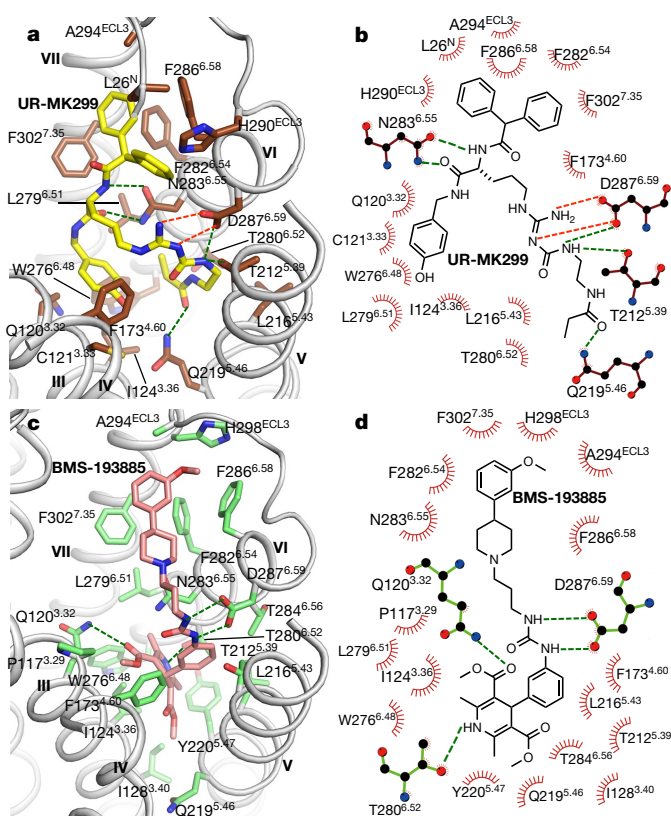


Fig. 2 | Ligand-binding pocket in Y₁R for UR-MK299 and BMS-193885. **a**, Binding pocket for UR-MK299. The receptor is shown in grey cartoon representation. UR-MK299 (yellow carbons) and receptor residues (dark brown carbons) involved in ligand binding are shown as sticks. Salt bridge and hydrogen bonds are shown as red and green dashed lines, respectively. **b**, Schematic representation of the interactions between Y₁R and UR-MK299 analysed using the LigPlot⁺ program³⁰. The stick drawing of Y₁R residues is coloured dark brown. **c**, Binding pocket for BMS-193885. BMS-193885 (pink carbons) and receptor residues (green carbons) involved in ligand binding are shown as sticks. **d**, Schematic representation of interactions between Y₁R and BMS-193885 analysed using the LigPlot⁺ program³⁰. The stick drawing of Y₁R residues is coloured green.

Y₁R antagonist was confirmed by the NPY-induced inositol phosphate accumulation of Y₁R when inhibited by UR-MK299 and several related Y₁R antagonists—BIBP3226, BIBO3304, UR-HU404 and UR-MK289 (Extended Data Fig. 1e–i). The F302^{7.35}A mutation abolishes the antagonistic activity for all these antagonists, and a two- to fivefold decrease in the antagonistic effect of all tested antagonists was observed for the F286^{6.58}A mutation (Fig. 3a–c, Extended Data Fig. 2 and Extended Data Table 2).

The hydroxyphenyl group of UR-MK299 sits in a groove formed by helices III and VI of the receptor, enabling hydrophobic contacts with residues Q120^{3.32}, C121^{3.33}, I124^{3.36}, W276^{6.48} and L279^{6.51}. In Y₁R and Y₂R, Q120^{3.32} is suggested to be the interaction partner for the C terminus of NPY and crucial for receptor activation¹⁶. In the Y₁R–UR-MK299 structure, this residue forms a hydrophobic contact with the phenyl ring of the hydroxyphenyl group in UR-MK299, potentially blocking the binding of Y₁R to NPY. Mutagenesis data show that the Q120^{3.32}N mutation does not influence the inhibitory effect of Y₁R antagonists on NPY signalling, but a mutation to histidine increases the antagonistic activity of these ligands (Fig. 3d, e and Extended Data Table 2), suggesting that an additional π -stacking interaction with the antagonist is beneficial at this position. The highly conserved residue W^{6.48} represents the 'toggle switch' and was suggested to trigger receptor activation through a conformational change in various GPCRs¹⁷. In the Y₁R–UR-MK299 structure, the residue W276^{6.48} is in a conformation that is similar to those observed in other inactive class A GPCR

structures and is distinct from their active-state conformations^{18,19}. The hydroxyphenyl group of UR-MK299 forms a hydrophobic contact with W276^{6.48}, potentially preventing its activation-related motion thus stabilizing the receptor in an inactive conformation. Compared to the wild-type receptor, the Y₁R mutant W276^{6.48}A displayed an over 2,000-fold decrease in its binding affinity to [³H]UR-MK299 (Extended Data Table 3) and reduced the antagonistic activity of the arginina-mide-type Y₁R antagonists by four- to sevenfold (Fig. 3f and Extended Data Table 2), supporting its important role in antagonist recognition.

Residues N283^{6.55} and D287^{6.59} were suggested as the most important amino acids for Y₁R ligand recognition²⁰. In the Y₁R–UR-MK299 structure, N283^{6.55} is engaged in two hydrogen bonds with the α -nitrogen and the carboxylic oxygen next to the hydroxybenzylamine moiety of UR-MK299. D287^{6.59} builds a salt bridge with the protonated guanidinyll moiety and a hydrogen bond with the carbamoyl group, in agreement with a decrease in antagonist affinity when the carbamoyl group was replaced by an alkoxy-carbonyl, acyl or alkyl group²¹. The mutants N283^{6.55}A and D287^{6.59}N displayed a notable loss of NPY-induced receptor function, a complete abolishment of antagonistic activity for the small-molecule antagonists (Fig. 3g, h and Extended Data Table 2), and an over 2,000-fold decrease in the binding affinity of Y₁R to [³H]UR-MK299 (Extended Data Table 3). These data indicate the critical roles of these two residues in agonist and antagonist binding. Additionally, the carbamoyl substituent at the guanidine group binds deep in a sub-pocket shaped by helices V and VI, characterized by hydrophobic contacts with L216^{5.43}, T280^{6.52} and N283^{6.55}, and a hydrogen bond between the oxygen of the propionyl group and Q219^{5.46}. The latter was reflected by a 30-fold decrease in the binding affinity of [³H]UR-MK299 to the Y₁R mutants Q219^{5.46}A and Q219^{5.46}V (Extended Data Table 3). Extra empty space at the bottom of the sub-pocket is observed in the Y₁R–UR-MK299 structure, suggesting that a larger substituent may be allowed (Extended Data Fig. 1c). This is supported by studies showing that other carbamoylated arginina-mide-type Y₁R antagonists containing longer carbamoyl chains, such as UR-MK136 (Extended Data Fig. 1j), bind to the receptor with a relatively high affinity¹⁰.

UR-MK299 was reported to exhibit high Y₁R selectivity (Y₂R, inhibition constant (K_i) > 3,000 nM; Y₄R and Y₅R, K_i > 10,000 nM) and specificity compared to two related neuropeptide FF (NPFF) receptors (NPFF₁R, K_i = 1,000 nM; NPFF₂R, K_i > 3,000 nM)¹⁰. Sequence alignment reveals that most of the key residues involved in UR-MK299 binding are conserved between Y₁R, the other NPY receptors and the NPFFRs, except for F^{4.60}, Q^{5.46}, N^{6.55} and F^{6.58} (Extended Data Fig. 3), indicating the importance of these four residues in terms of the selectivity and specificity of UR-MK299. Y₂R is the only NPY receptor with L^{5.46} instead of Q^{5.46}, preventing key polar contacts. In Y₄R, E^{6.58} disturbs the F^{6.54}–F^{6.58}–F^{7.35} hydrophobic patch and probably mediates selectivity, supported by the F^{6.58}E mutation in Y₁R reducing binding affinity for BIBP3226²², which contains the same diphenylmethyl group as UR-MK299. Similarly, hydrophilic residues at key positions impede high-affinity binding at Y₅R (T^{6.58}) and NPFF₂R (S^{6.58}), while the hydrophobic pocket is preserved in NPFF₁R (L^{6.54}–I^{6.58}–F^{7.35}), although with less bulk, leading to a moderate affinity of BIBP3226 (K_i = 18 nM)¹⁰.

The ligands BMS-193885 and UR-MK299 occupy a similar binding pocket within the helical bundle of Y₁R (Fig. 2c, d and Extended Data Fig. 1k). The dihydropyridine group of BMS-193885 fits in a sub-pocket formed by helices III, V and VI, which aligns with previous structure–activity relationship studies showing that larger substituents at position three of the dihydropyridine ring reduced Y₁R binding affinity²³. Residue T280^{6.52} forms a hydrogen bond with the nitrogen of the dihydropyridine ring as confirmed by our mutagenesis studies, which showed that the T280^{6.52}A mutation decreased the binding affinity of BMS-193885 by about 330-fold (Extended Data Table 3), in agreement with a reported lower affinity *N*-methylated derivative²⁴. Additionally, the dihydropyridine ring makes a hydrophobic contact with residue I124^{3.36}, which is consistent with a 400-fold decrease in

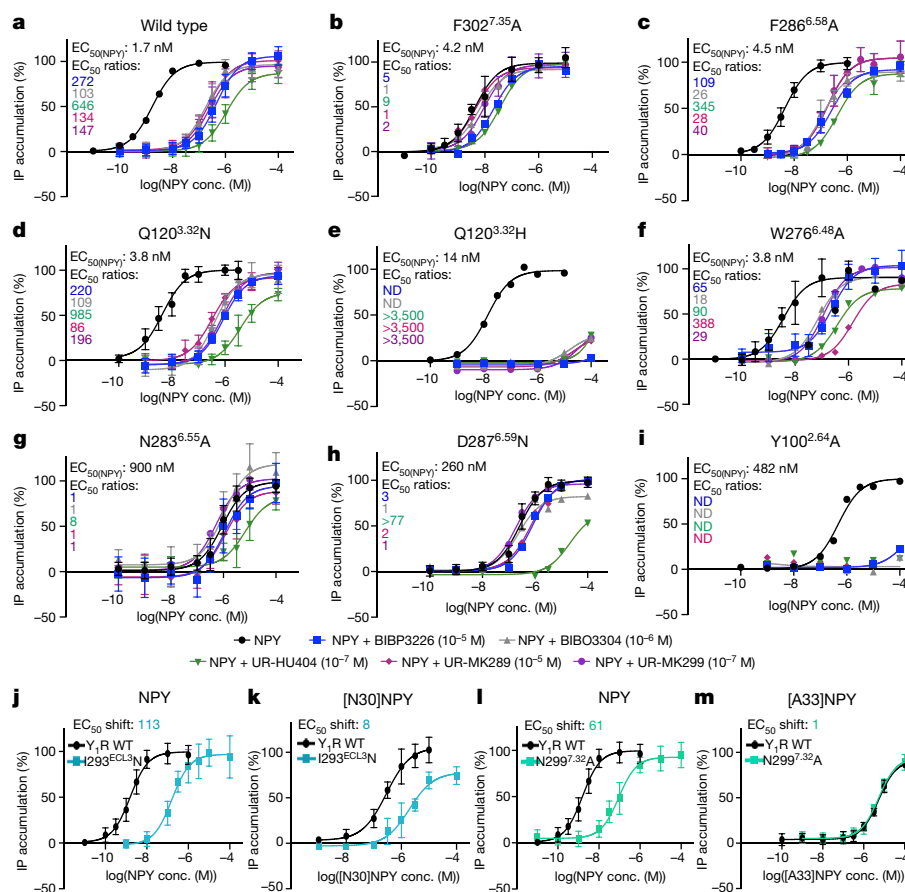


Fig. 3 | Inositol phosphate accumulation assays. a–i, NPY-induced inositol phosphate (IP) accumulation of wild-type (WT) and mutant Y_1 receptors in the absence of antagonists or in the presence of BIBP3226 (10^{-5} M), BIBO3304 (10^{-6} M), UR-HU404 (10^{-7} M), UR-MK289 (10^{-5} M) or UR-MK299 (10^{-7} M). EC_{50} values of NPY (black) and EC_{50} ratios ($EC_{50}(\text{NPY} + \text{antagonist})/EC_{50}(\text{NPY})$) for antagonists (coloured) are given in the top left corner for each plot. A reduced EC_{50} ratio of the mutant compared to the wild-type receptor was interpreted as important for the respective antagonist. ND, not determined; NPY conc., concentration of NPY. **j–m**, Complementary mutagenesis assays of [N30]NPY with I293^{ECL3}N

(**j, k**) and [A33]NPY with N299^{7.32}A (**l, m**). EC_{50} shifts ($EC_{50}(\text{mutant})/EC_{50}(\text{wild type})$) are given in the top left corner for each plot. A reduced EC_{50} shift of the NPY analogue/ Y_1 R mutant compared to the NPY/ Y_1 R mutant was interpreted as no further loss of function and a direct interaction between both positions. At least two independent experiments were performed in technical duplicates. Where more than two experiments were performed (**a–d, f–h, j–m**), data are shown as mean \pm s.e.m. Where two experiments were performed (**e, i**), data from a representative experiment are shown. See Extended Data Table 2 for detailed statistical evaluation.

the affinity of the mutant I124^{3.36}A (Extended Data Table 3). It was also reported that methylation of either nitrogen of the urea group of BMS-193885 decreased the binding ability of the methylated derivatives to Y_1 R²⁴, suggesting that these hydrogen bond donors are critical for Y_1 R recognition. Indeed, in the BMS-193885-bound Y_1 R structure, the urea group forms hydrogen bond interactions with D287^{6.59}. Similar to the diphenylmethyl group of UR-MK299, the piperidine and methoxyphenyl rings of BMS-193885 form extensive hydrophobic contacts with the residues F282^{6.54}, F286^{6.58} and F302^{7.35}. Replacement of the methoxyphenyl substituent by piperidine resulted in lower binding affinity to Y_1 R²³, indicating the importance of the methoxyphenyl group in Y_1 R binding and reflecting lipophilic demands at this position.

Understanding the binding mode of the endogenous agonist NPY at a molecular level will facilitate the rational development of Y_1 R-selective ligands. The C-terminal pentapeptide of NPY was found to be essential for binding to the NPY receptors²⁵. Because the hydroxyphenyl and the argininamide group of UR-MK299 mimic R35 and Y36 in the C terminus of NPY (Extended Data Fig. 11), the crystal structure of Y_1 R–UR-MK299 serves as a good template for molecular docking of the agonist. To aid docking, complementary mutagenesis studies were performed to determine corresponding interaction partners between Y_1 R and NPY (Extended Data Table 4a). Furthermore, solid-state nuclear magnetic resonance (NMR) chemical shift measurements revealed residue-specific alterations of the secondary structure of NPY

upon binding to Y_1 R (Extended Data Fig. 4). Several key Y_1 R–NPY contacts identified by the mutagenesis studies were used to guide NPY docking in Rosetta²⁶ with the final models being filtered against the NMR data to generate a final ensemble that best represents the combined data. The NPY-bound model reveals a relatively flat NPY– Y_1 R binding pose with the C-terminal tetrapeptide R33–Y36, identified as either a random coil or a β -strand structure in NMR, penetrating into the binding pocket (Fig. 4a). The unstructured N terminus (Y1–P13) is in close proximity to the second extracellular loop (ECL2), while the α -helix in the middle region of NPY (A14–T32) lies along ECL1 and ECL3 and points away from ECL2.

Inspection of the binding pocket of NPY reveals that the binding pose of residue R35 of NPY is similar to that of the argininamide of UR-MK299 (Fig. 4b). R35 forms a salt bridge with the D287^{6.59} residue of Y_1 R and approaches N283^{6.55} (Fig. 4c). The NPY mutant R35A displays a decrease in activity of over 6,000-fold, which represents the highest influence on agonist potency of all tested NPY analogues (Extended Data Table 4a), supporting the importance of the positively charged residue in NPY recognition. Aspartate or glutamate residues are not found at position 6.59 in any peptide GPCRs except for the receptors that bind to Arg–Phe–amide peptides, including NPFF, prolactin-releasing peptide and pyroglutamylated Arg–Phe–amide peptide, which share a common C-terminal Arg–Phe–NH₂ motif, supporting the hypothesis that the arginine residue may function in a manner that

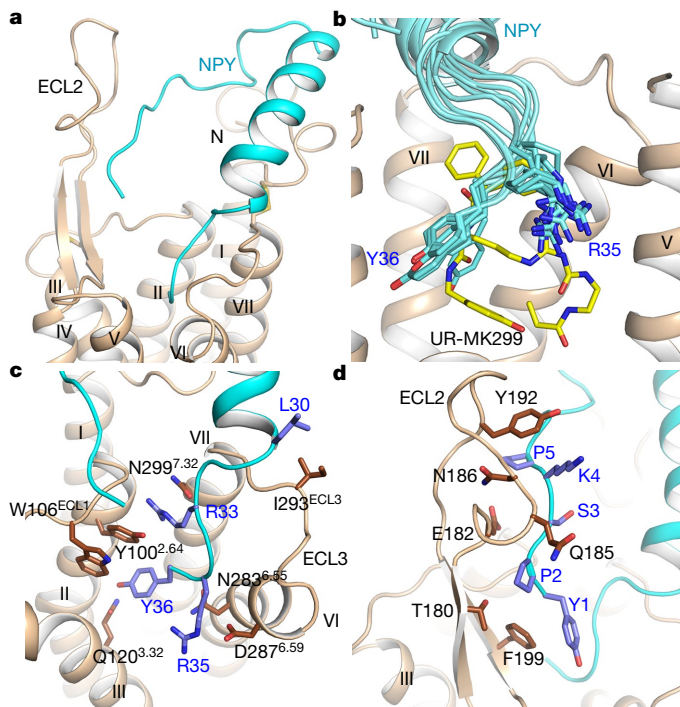


Fig. 4 | Docking poses of NPY. **a**, Predicted NPY binding pose. The receptor and the lowest energy NPY conformation are shown as cartoons, and are coloured brown and cyan, respectively. **b**, Comparison of UR-MK299 (yellow sticks) binding mode and predicted ensemble binding mode of residues R35 and Y36 of NPY (cyan sticks). **c**, Predicted binding mode between Y_1R and the C terminus of NPY. Key residues involved in the Y_1R -NPY interaction are shown as sticks and coloured dark brown (Y_1R) and blue (NPY). **d**, Predicted binding mode between ECL2 of Y_1R and the N terminus of NPY. Residues in the ECL2 of Y_1R and the N terminus of NPY that may form contacts are shown as dark brown and blue sticks, respectively.

is similar to that of the R35 of NPY by interacting with the conserved D/E^{6.59} of the respective receptors²⁷. In contrast to the similarity between the binding modes of the R35 of NPY and the guanidine group of UR-MK299, the C-terminal tyrosinamide of NPY and the hydroxyphenyl group of UR-MK299 show different orientations. The hydroxyphenyl ring is oriented towards helix V (Q219^{5,46}) in the UR-MK299-bound Y_1R structure, whereas Y36 of NPY points towards the Q120^{3,32} residue on helix III in the NPY-docked model (Fig. 4c). This may arise from the opposite configuration of the stereo centre in the R35 of NPY and UR-MK299, as well as by only partial mimicking of the Y36-NH₂ of NPY by a 4-hydroxybenzyl group in UR-MK299 (Extended Data Fig. 1g, l). In the Y_1R -UR-MK299 structure, residue Q120^{3,32} forms a hydrophobic contact with the hydroxyphenyl group of the antagonist. By contrast, the NPY-bound model shows that the side chain of Q120^{3,32} points almost in the opposite direction and engages in a hydrogen bond with the hydroxy group of Y36-NH₂ (Extended Data Fig. 1d), in a similar manner to the previously suggested interaction between the Y_2R residue Q^{3,32} and NPY²⁸. In Y_2R , it was also reported that Q^{3,32} may interact with the C-terminal amide of NPY¹⁶. Inositol phosphate accumulation studies show that the Y_1R mutation Q120^{3,32}H leads to a 26-fold decrease in the potency of NPY, and NPY-tyramide lacking the C-terminal amide displays a 45-fold loss of activity. Complementary mutagenesis analysis revealed an additional reduction of NPY-tyramide potency at the Q120^{3,32}H mutant, and thus rules out a direct contact between the C-terminal amide of NPY and Q120^{3,32} in Y_1R (Extended Data Table 4a). Additionally, Y36 of NPY forms hydrophobic contacts with Y100^{2,64} and W106^{ECL1} in Y_1R (Fig. 4c). Although Y100^{2,64} is not involved in antagonist binding, mutagenesis data suggest a critical role in agonist recognition as the Y_1R mutant Y100^{2,64}A displays a

284-fold decrease in potency for NPY (Fig. 3i and Extended Data Table 2). Furthermore, the model reveals close contacts between L30 of NPY and I293 in ECL3 of Y_1R and between R33 of NPY and the Y_1R residue N299^{7,32} (Fig. 4c), which align with complementary mutagenesis data showing no further loss of function for combining mutant I293N with [N30]NPY and N299^{7,32}A with [A33]NPY (Fig. 3j–m and Extended Data Table 4a).

Previous studies have shown that different NPY receptors behave differently when binding to the N terminus of NPY. Y_2R and Y_5R can bind to N-terminally truncated NPY, whereas Y_1R and Y_4R require the complete N terminus of NPY for full agonist potency^{25,27}. However, these data did not allow conclusions about the interaction of the N terminus of NPY with the receptor. To further explore the involvement of the NPY N terminus in recognition between the receptor and ligand, we performed mutagenesis studies, showing that truncation of the first two residues of NPY (NPY(3–36)) reduces peptide potency by more than 50-fold (Extended Data Table 4b). This decrease in potency, however, is not seen when these residues are mutated to alanine ([A1,A2]NPY, fivefold shift in the half-maximal effective concentration (EC₅₀)), suggesting important contributions of the peptide backbone in binding to the receptor. Our NPY-bound model suggests that the N-terminal region of NPY makes close contacts with the T180–F199 fragment in ECL2 of Y_1R and is also in proximity to the receptor N terminus (Fig. 4a, d). To experimentally verify interacting sites in the receptor, we performed photo-crosslinking studies between NPY analogues carrying the highly reactive *p*-benzoyl-phenylalanine [Bpa¹, K⁴[(Ahx)₂-biotin]]NPY (in which Ahx denotes aminohexanoate) and Y_1R . Crosslinked fragments were assigned to two regions in Y_1R , the N terminus (K21–D32) and the ECL2 (A191–D205) (Extended Data Fig. 5 and Extended Data Table 5). Previous studies demonstrated that deletion of the Y_1R N terminus does not interfere with receptor signalling, but reduces NPY binding by about 95% compared to the full-length receptor²⁹. This creates the possibility that the N terminus of Y_1R has a role in recognizing and positioning the peptide ligand, which is in agreement with the photo-crosslinking data. Consistent with the crosslinking hits in receptor ECL2, our mutagenesis data show that the F184A/N and V197N mutations in this region greatly reduce NPY potency (Extended Data Table 4c). Together, these data suggest that the N terminus and ECL2 of Y_1R have important roles in the recognition of the N terminus of NPY and receptor activation. This contrasts with NPY binding at Y_2R , in which ECL2 may interact with the central α -helix of NPY and the peptide N terminus is flexible and not anchored by the receptor¹⁶. Although this study provides insights into the interactions between Y_1R and NPY, further structural details, such as the structures of Y receptors bound to NPY, are required to fully understand the endogenous agonist-binding modes of the NPY receptor family.

Online content

Any Methods, including any statements of data availability and Nature Research reporting summaries, along with any additional references and Source Data files, are available in the online version of the paper at <https://doi.org/10.1038/s41586-018-0046-x>.

Received: 20 July 2017; Accepted: 16 March 2018;

Published online: 18 April 2018

- Zhang, L., Bijker, M. S. & Herzog, H. The neuropeptide Y system: pathophysiological and therapeutic implications in obesity and cancer. *Pharmacol. Ther.* **131**, 91–113 (2011).
- Morales-Medina, J. C., Dumont, Y. & Quirion, R. A possible role of neuropeptide Y in depression and stress. *Brain Res.* **1314**, 194–205 (2010).
- Michel, M. C. et al. XVI. International Union of Pharmacology recommendations for the nomenclature of neuropeptide Y, peptide YY, and pancreatic polypeptide receptors. *Pharmacol. Rev.* **50**, 143–150 (1998).
- Yulyaningsih, E., Zhang, L., Herzog, H. & Sainsbury, A. NPY receptors as potential targets for anti-obesity drug development. *Br. J. Pharmacol.* **163**, 1170–1202 (2011).
- Sousa, D. M., Herzog, H. & Lamghari, M. NPY signalling pathway in bone homeostasis: Y1 receptor as a potential drug target. *Curr. Drug Targets* **10**, 9–19 (2009).

6. Antal-Zimanyi, I. et al. Pharmacological characterization and appetite suppressive properties of BMS-193885, a novel and selective neuropeptide Y₁ receptor antagonist. *Eur. J. Pharmacol.* **590**, 224–232 (2008).
7. Leibowitz, S. F., Sladek, C., Spencer, L. & Tempel, D. Neuropeptide Y, epinephrine and norepinephrine in the paraventricular nucleus: stimulation of feeding and the release of corticosterone, vasopressin and glucose. *Brain Res. Bull.* **21**, 905–912 (1988).
8. MacNeil, D. J. NPY Y₁ and Y₅ receptor selective antagonists as anti-obesity drugs. *Curr. Top. Med. Chem.* **7**, 1721–1733 (2007).
9. Reubi, J. C., Gugger, M., Waser, B. & Schaefer, J. C. Y₁-mediated effect of neuropeptide Y in cancer: breast carcinomas as targets. *Cancer Res.* **61**, 4636–4641 (2001).
10. Keller, M. et al. N^ω-carbamoylation of the argininamide moiety: an avenue to insurmountable NPY Y₁ receptor antagonists and a radiolabeled selective high-affinity molecular tool ([³H]UR-MK299) with extended residence time. *J. Med. Chem.* **58**, 8834–8849 (2015).
11. White, J. F. et al. Structure of the agonist-bound neurotensin receptor. *Nature* **490**, 508–513 (2012).
12. Yin, J. et al. Structure and ligand-binding mechanism of the human OX₁ and OX₂ orexin receptors. *Nat. Struct. Mol. Biol.* **23**, 293–299 (2016).
13. Yin, J., Mobarec, J. C., Kolb, P. & Rosenbaum, D. M. Crystal structure of the human OX₂ orexin receptor bound to the insomnia drug suvorexant. *Nature* **519**, 247–250 (2015).
14. Shihoya, W. et al. Activation mechanism of endothelin ET_B receptor by endothelin-1. *Nature* **537**, 363–368 (2016).
15. Ballesteros, J. A. & Weinstein, H. in *Methods in Neurosciences* Vol. 25 (ed. S. Sealfon) 366–428 (Elsevier, Amsterdam, 1995).
16. Kaiser, A. et al. Unwinding of the C-terminal residues of neuropeptide Y is critical for Y₂ receptor binding and activation. *Angew. Chem. Int. Edn Engl.* **54**, 7446–7449 (2015).
17. Venkatakrisnan, A. J. et al. Molecular signatures of G-protein-coupled receptors. *Nature* **494**, 185–194 (2013).
18. Rasmussen, S. G. et al. Crystal structure of the β₂ adrenergic receptor-Gs protein complex. *Nature* **477**, 549–555 (2011).
19. Standfuss, J. et al. The structural basis of agonist-induced activation in constitutively active rhodopsin. *Nature* **471**, 656–660 (2011).
20. Sautel, M. et al. Neuropeptide Y and the nonpeptide antagonist BIBP 3226 share an overlapping binding site at the human Y₁ receptor. *Mol. Pharmacol.* **50**, 285–292 (1996).
21. Keller, M. et al. Guanidine-acylguanidine bioisosteric approach in the design of radioligands: synthesis of a tritium-labeled N^ω-propionylargininamide ([³H]-UR-MK114) as a highly potent and selective neuropeptide Y₁ receptor antagonist. *J. Med. Chem.* **51**, 8168–8172 (2008).
22. Sjödin, P. et al. Re-evaluation of receptor-ligand interactions of the human neuropeptide Y receptor Y₁: a site-directed mutagenesis study. *Biochem. J.* **393**, 161–169 (2006).
23. Poindexter, G. S. et al. Dihydropyridine neuropeptide Y Y₁ receptor antagonists. *Bioorg. Med. Chem. Lett.* **12**, 379–382 (2002).
24. Poindexter, G. S. et al. Dihydropyridine neuropeptide Y Y₁ receptor antagonists 2: bioisosteric urea replacements. *Bioorg. Med. Chem.* **12**, 507–521 (2004).
25. Pedragosa-Badia, X., Stichel, J. & Beck-Sickingler, A. G. Neuropeptide Y receptors: how to get subtype selectivity. *Front. Endocrinol. (Lausanne)* **4**, 5 (2013).
26. Bender, B. J. et al. Protocols for molecular modeling with Rosetta3 and RosettaScripts. *Biochemistry* **55**, 4748–4763 (2016).
27. Merten, N. et al. Receptor subtype-specific docking of Asp⁶⁵⁹ with C-terminal arginine residues in Y receptor ligands. *J. Biol. Chem.* **282**, 7543–7551 (2007).
28. Xu, B. et al. Mutagenesis and computational modeling of human G-protein-coupled receptor Y₂ for neuropeptide Y and peptide YY. *Biochemistry* **52**, 7987–7998 (2013).
29. Lindner, D., Walther, C., Tennemann, A. & Beck-Sickingler, A. G. Functional role of the extracellular N-terminal domain of neuropeptide Y subfamily receptors in membrane integration and agonist-stimulated internalization. *Cell. Signal.* **21**, 61–68 (2009).
30. Laskowski, R. A. & Swindells, M. B. LigPlot⁺: multiple ligand-protein interaction diagrams for drug discovery. *J. Chem. Inf. Model.* **51**, 2778–2786 (2011).

Acknowledgements We are grateful to T. Zellmann for his contribution to the modelling in the early state of the project and for the technical support of R. Reppich-Sacher (mass spectrometry) and K. Löbner (cell culture). We thank H. A. Scheidt for support with solid-state NMR measurements and M. Beer-Krön, D. Fritsch, S. Bollwein and B. Wenzl for expert help in performing radioligand-binding experiments. The synchrotron radiation experiments were performed at the BL41XU of SPring-8 with approval of the Japan Synchrotron Radiation Research Institute (proposal no. 2015B2026, 2015B2027, 2016A2517, 2016A2518, 2016B2517 and 2016B2518). We thank the beamline staff members K. Hasegawa, H. Okumura, N. Mizuno, T. Kawamura and H. Murakami of the BL41XU for help with X-ray data collection. This work was supported by CAS Strategic Priority Research Programs XDB08020000 (B.W.) and XDB08030102 (R.Z.), the Key Research Program of Frontier Sciences, CAS, Grant no. QYZDB-SSW-SMC024 (B.W.) and QYZDB-SSW-SMC054 (Q.Z.), the National Science Foundation of China grants 31570739 (B.W.), 81525024 (Q.Z.), 3170040264 (Z.Y.) and 31470792 (S.Y.), Program of Shanghai Academic/Technology Research Leader no. 18XD1404800 (Z.Y., Q.Z.), the European Community, the Free State of Saxony (SAB 100148835 to D.H. and 100881433 to A.G.B.-S.) and the Deutsche Forschungsgemeinschaft (DFG) (Be1264-16, SFB 1052/A3, research grant KE 1857/1-1 and Graduate Training Program GRK 1910). Work in the Meiler laboratory is supported by the NIH (R01 GM080403, R01 DK097376, R01 HL122010) and NSF (CHE 1305874).

Reviewer information Nature thanks N. Holliday and the other anonymous reviewer(s) for their contribution to the peer review of this work.

Author contributions Z.Y. and S.H. optimized the construct, developed the purification procedure, purified the Y₁R protein for crystallization, performed crystallization trials, solved the structures and wrote the manuscript. M.K., D.W., G.B., N.P. and T.L. synthesized the compounds, designed, performed and analysed the ligand-binding assay. A.K., K.B. and L.M.K. performed peptide synthesis, inositol phosphate accumulation assays, the photo-crosslinking assay and mass spectrometry after crosslinking. B.J.B. helped to refine the Y₁R-UR-MK299 structure and modelled the Y₁R-NPY complex. M.B. and P.S. performed NMR analysis and analysed NMR data. C.Y. expressed the Y₁R proteins. B.L. helped with construct and crystal optimization. S.Y., R.Z., B.X., D.L., R.C.S., D.H., J.M., A.G.B.-S. and A.B. helped with structure analysis, interpretation and edited the manuscript. R.C.S. helped to initiate the project. D.H. oversaw NMR studies. J.M. oversaw molecular docking. Q.Z. collected X-ray diffraction data and solved the structures. A.G.B.-S. oversaw peptide synthesis, inositol phosphate accumulation and photo-crosslinking assays. A.B. oversaw compound synthesis and ligand-binding assays. B.W. and Q.Z. initiated the project, planned and analysed experiments, supervised the research and wrote the manuscript with input from all co-authors.

Competing interests The authors declare no competing interests.

Additional information

Extended data is available for this paper at <https://doi.org/10.1038/s41586-018-0046-x>.

Supplementary information is available for this paper at <https://doi.org/10.1038/s41586-018-0046-x>.

Reprints and permissions information is available at <http://www.nature.com/reprints>.

Correspondence and requests for materials should be addressed to M.K., A.G.B. or B.W.

Publisher's note: Springer Nature remains neutral with regard to jurisdictional claims in published maps and institutional affiliations.

METHODS

No statistical methods were used to predetermine sample size. The experiments were not randomized and the investigators were not blinded to allocation during experiments and outcome assessment.

Cloning and protein expression. The DNA sequence of wild-type human Y_1R was optimized and synthesized by Genewiz and then cloned into a modified pFastBac1 vector (Invitrogen), which contains an expression cassette with a haemagglutinin signal sequence followed by a Flag tag before the receptor at the N terminus and a PreScission protease site followed by a $10 \times$ His-tag at the C terminus. An engineered construct was generated by inserting a modified T4 lysozyme (T4L)³¹ at the third intracellular loop (ICL3) between residues R241 and D250 and introducing a mutation (F129^{3,41W})³². Twenty-five amino acids (V359–I384) were truncated at the C terminus to further improve protein yield and stability. Bac-to-Bac Baculovirus Expression System (Invitrogen) was used to generate high-titre ($> 10^8$ viral particles per ml) recombinant baculovirus. *Spodoptera frugiperda* (Sf9) cells (Invitrogen) at a density of 2×10^6 cells per ml were infected by viral stock at an MOI (multiplicity of infection) of 5. As well as the virus, a ligand (UR-MK299 or BMS-193885) was added to the cell culture to a final concentration of $1 \mu\text{M}$. Transfected cells were cultured at 27°C for 48 h and then collected by centrifugation and stored at -80°C until use.

Purification of Y_1R -UR-MK299 and Y_1R -BMS-193885 complexes. Frozen insect cells expressing the Y_1R -UR-MK299 complex were disrupted with thawing and repeated dounce homogenization in a hypotonic buffer containing 10 mM HEPES, pH 7.5, 10 mM MgCl_2 , 20 mM KCl and protease inhibitor cocktail (Roche). After centrifugation at $160,000g$ for 30 min, cell debris was re-suspended in a high-osmotic buffer (10 mM HEPES, pH 7.5, 1 M NaCl, 10 mM MgCl_2 , 20 mM KCl) and then homogenized extensively. Soluble and membrane associated proteins were removed from the suspension by centrifugation. This procedure was repeated two to three more times and then the hypotonic buffer was used to remove the high concentration of NaCl. Purified membranes were re-suspended in the hypotonic buffer with additional 30% (v/v) glycerol and stored at -80°C until use.

Purified membranes were thawed on ice in the presence of $100 \mu\text{M}$ UR-MK299, 2 mg ml^{-1} iodoacetamide (Sigma) and EDTA-free protease inhibitor cocktail (Roche) and incubated at 4°C for 1 h. Equal volume of solubilization buffer containing 100 mM HEPES, pH 7.5, 1 M NaCl, 1% (w/v) *n*-dodecyl- β -D-maltopyranoside (DDM, Anatrace), 0.2% (w/v) cholesterol hemisuccinate (CHS, Sigma) was added and incubation was continued for an additional 3 h. The supernatant was isolated by centrifugation at $160,000g$ for 30 min and incubated with TALON resin (Clontech) supplemented with 10 mM imidazole, pH 7.5 at 4°C overnight. The resin was first washed with ten column volumes of 25 mM HEPES, pH 7.5, 500 mM NaCl, 0.05% (w/v) DDM, 0.01% (w/v) CHS, 10% (v/v) glycerol, 30 mM imidazole and $50 \mu\text{M}$ UR-MK299, then with ten column volumes of 50 mM HEPES, pH 7.5, 500 mM NaCl, 0.05% (w/v) DDM, 0.01% (w/v) CHS, 10% (v/v) glycerol, 10 mM MgCl_2 , 5 mM ATP and $50 \mu\text{M}$ UR-MK299 and finally with five column volumes of 25 mM HEPES, pH 7.5, 500 mM NaCl, 0.05% (w/v) DDM, 0.01% (w/v) CHS, 10% (v/v) glycerol and $50 \mu\text{M}$ UR-MK299. The protein was eluted by five column volumes of 25 mM HEPES, pH 7.5, 500 mM NaCl, 0.05% (w/v) DDM, 0.01% (w/v) CHS, 10% (v/v) glycerol, 300 mM imidazole and $100 \mu\text{M}$ UR-MK299. A PD MiniTrap G-25 column (GE healthcare) was used to remove imidazole. The C-terminal His-tag and glycosylation was then treated by overnight digestion with His-tagged PreScission protease (custom-made) and His-tagged PNGase F (custom-made). Ni-NTA super flow resin (Qiagen) reverse binding was performed to remove the PreScission protease, PNGase F and the cleaved His-tag. The purified Y_1R -UR-MK299 complex was collected and concentrated to 20 – 30 mg ml^{-1} with a 100 kDa molecular mass cut-off concentrator (Sartorius Stedim Biotech). Receptor purity and monodispersity were estimated by SDS-PAGE and analytical size-exclusion chromatography.

The Y_1R -BMS-193885 complex protein was purified following the same procedure as above. The membranes of the Y_1R construct were incubated with $50 \mu\text{M}$ BMS-193885, 2 mg ml^{-1} iodoacetamide (Sigma), and EDTA-free protease inhibitor cocktail (Roche) at 4°C for 1 h, and then solubilized in final concentration of 50 mM HEPES, pH 7.5, 500 mM NaCl, 0.5% (w/v) DDM, 0.1% (w/v) CHS, 10% glycerol and $25 \mu\text{M}$ BMS-193885 at 4°C for 3 h. The solubilized Y_1R -BMS-193885 complex bound to the TALON resin was first washed with ten column volumes of 25 mM HEPES, pH 7.5, 500 mM NaCl, 0.05% (w/v) DDM, 0.01% (w/v) CHS, 10% (v/v) glycerol, 30 mM imidazole and $25 \mu\text{M}$ BMS-193885, and then with ten column volumes of 50 mM HEPES, pH 7.5, 500 mM NaCl, 0.05% (w/v) DDM, 0.01% (w/v) CHS, 10% (v/v) glycerol, 10 mM MgCl_2 , 5 mM ATP and $25 \mu\text{M}$ BMS-193885 and finally with five column volumes of 25 mM HEPES, pH 7.5, 500 mM NaCl, 0.05% (w/v) DDM, 0.01% (w/v) CHS, 10% (v/v) glycerol and $25 \mu\text{M}$ BMS-193885. The protein was eluted by five column volumes of 25 mM HEPES, pH 7.5, 500 mM NaCl, 0.05% (w/v) DDM, 0.01% (w/v) CHS, 10% (v/v) glycerol, 300 mM imidazole and $50 \mu\text{M}$ BMS-193885. The eluted sample was concentrated and desalted using the PD MiniTrap G-25 column (GE healthcare). Overnight

digestion by PreScission protease and PNGase F and Ni-NTA reverse binding were then performed to further purify the protein. The complex protein was concentrated to 10 – 20 mg ml^{-1} and analysed by SDS-PAGE and analytical size-exclusion chromatography.

Lipidic cubic phase crystallization of antagonist-bound Y_1R receptors. The Y_1R sample in complex with UR-MK299 or BMS-193885 was mixed with molten lipid (monoolein and cholesterol 10:1 by mass) at a weight ratio of 1:1.5 (protein:lipid) using two syringes to create a lipidic cubic phase (LCP). The mixture was dispensed onto glass sandwich plates (Shanghai FAlst BioTech) in 40 nl drop and overlaid with 800 nl precipitant solution using a Gryphon robot (Art-Robbins). Protein reconstitution in LCP and crystallization trials were performed at room temperature (19 – 22°C). Plates were placed in an incubator (Rock Imager, Formulatrix) and imaged at 20°C automatically following a schedule. Crystals of Y_1R -UR-MK299 complex appeared after 4 days and grew to full size ($150 \times 50 \times 5 \mu\text{m}^3$) within two weeks in 0.1 M Tris, pH 7.4–8.0, 30–40% (v/v) PEG400, 50–150 mM sodium tartrate and $100 \mu\text{M}$ UR-MK299. The Y_1R -BMS-193885 complex was crystallized in 0.1 M HEPES, pH 7.2–7.6, 20% PEG400 and $50 \mu\text{M}$ BMS-193885 with the maximum size of $30 \times 10 \times 5 \mu\text{m}^3$. The crystals of Y_1R -UR-MK299 and Y_1R -BMS-193885 complexes were harvested directly from LCP using $150 \mu\text{m}$ and $50 \mu\text{m}$ micro mounts (M2-L19-50/100, MiTeGen), respectively, and flash frozen in liquid nitrogen.

Data collection and structure determination. X-ray diffraction data were collected at the SPring-8 beam line 41XU, Hyogo, Japan, on a Pilatus3 6M detector (X-ray wavelength 1.0000 \AA). Crystals were exposed with a $10 \mu\text{m} \times 8 \mu\text{m}$ mini-beam for 0.2 s and 0.2° oscillation per frame. Data from the 47 best-diffracting crystals of the Y_1R -UR-MK299 complex and 33 crystals of the Y_1R -BMS-193885 complex were processed by XDS³³. The structure of the Y_1R -UR-MK299 complex was solved by molecular replacement implemented in Phaser³⁴ using the receptor portion of NTS1 (Protein Data Bank (PDB) accession number 4GRV), converted to polyalanines, and T4L structure (PDB accession number 1C6P) as search models. The correct molecular replacement solution contained one Y_1R -T4L molecule in the asymmetric unit. Initial refinement was performed with REFMAC5³⁵ and BUSTER³⁶, and then manual examination and rebuilding of the refined coordinates were carried out in COOT³⁷ using both $|2F_o - |F_c||$ and $|F_o| - |F_c|$ maps. The structure has been carefully refined and the Ramachandran plot analysis indicates that 100% of the residues are in favourable (95.5%) or allowed (4.5%) regions (no outliers). The final model includes 306 residues (F18–R241 and S256–F337) of the 384 residues of Y_1R and residues N2–Y161 of T4L. The Y_1R -BMS-193885 complex structure was solved using Y_1R in the Y_1R -UR-MK299 complex and T4L as search models and refined using the same procedure. The Ramachandran plot analysis indicates that 100% of the residues are in favourable (95.4%) or allowed (4.6%) regions (no outliers). The final model of the Y_1R -BMS-193885 complex contains 301 residues (D31–R241 and D250–D339) of Y_1R and the 160 residues of T4L. Helix VIII in the Y_1R -UR-MK299 structure rotates towards helix VI by about 90° compared to the BMS-193885-bound structure, this is probably caused by crystal packing (Extended Data Fig. 1).

Immunoblotting. The total solubilized protein of the Sf9 membrane preparations (see above) used in the radio ligand binding assay was determined using the Bradford method according to the manufacturers' protocol (BioRad Protein Assay; BioRad). Aliquots of homogenized membrane preparations, corresponding to $100 \mu\text{g}$ of protein, were centrifuged at $50,000g$ at 4°C for 15 min, and the pellets were re-suspended in 50 mM Tris, pH 7.4, supplemented with 1 mM EDTA and protease inhibitors (SIGMAFAST Protease Inhibitor cocktail tablets, Sigma) at a protein concentration of $1,600 \mu\text{g ml}^{-1}$. Membrane homogenates ($15 \mu\text{l}$) were processed and subjected to immunoblotting as described previously³⁸ with the following modifications: blotting onto the nitrocellulose membrane was performed at 60 mA for 60 min. Primary antibody anti-Flag M1 from mouse (Sigma, F3040, lot SLBK1592V) was diluted 1:500. The secondary antibody, an anti-mouse IgG horseradish peroxidase (HRP)-conjugated antibody from goat (Sigma, A0168, lot 080M4839) was diluted 1:80,000. The washing steps after incubation with the primary and the secondary antibody were $3 \times 10 \text{ min}$ each. Control experiments in the absence of the primary antibody were not performed.

Radioligand-binding assay. All binding experiments with [^3H]UR-MK299 (synthesis described elsewhere¹⁰) were performed on Sf9 membrane preparations in PP 96-well microplates (Greiner Bio One) at $23 \pm 1^\circ\text{C}$ using a sodium-containing, iso-osmotic HEPES buffer (10 mM HEPES, pH 7.4, 150 mM NaCl, 5 mM KCl, 2.5 mM CaCl_2 , 1.2 mM KH_2PO_4 , 1.2 mM Mg_2SO_4 and 25 mM NaHCO_3 supplemented with 1% BSA) for competition-binding studies with antagonists, and a sodium-free, hypo-osmotic HEPES buffer (25 mM HEPES, pH 7.4, 2.5 mM CaCl_2 and 1 mM MgCl_2 supplemented with 1% BSA) for competition binding studies with the agonist NPY (hereafter, both buffers are referred to as 'binding buffer'). Before competition binding experiments, dissociation constant (K_d) values of [^3H]UR-MK299 were determined by saturation binding using the respective binding buffer. In the case of saturation-binding experiments, [^3H]UR-MK299 was 1:1

diluted with 'cold' UR-MK299 (hereafter, the mixture is referred to as 'radioligand'). On the day of the experiment, Sf9 membranes were thawed, re-suspended using a 1-ml syringe equipped with a needle (20 G) and then centrifuged at 16,000g at 4 °C for 10 min. The supernatant was discarded and the pellets were re-suspended in binding buffer using a 1-ml syringe equipped with a needle (27G3/4). The membrane homogenates were stored on ice until use. The total amount of protein per well was between 0.25 and 8 µg, depending on the receptor expression level.

Saturation binding experiments. For the determination of total binding, wells were pre-filled with binding buffer (160 µl), and then 20 µl of binding buffer, containing the radioligand at a concentration tenfold higher than the final concentration, was added. For the determination of unspecific binding (in the presence of UR-MK299 at a 100-fold excess), wells were pre-loaded with binding buffer (140 µl), binding buffer (20 µl) containing UR-MK299 (tenfold concentrated) and binding buffer (20 µl) containing the radioligand (tenfold concentrated). To all wells, 20 µl of the membrane suspension were added, and the plates were shaken at 23 °C for 90 min. The membranes were collected on GF/C filter mats (0.26 mm; Whatman) (pre-treated with 0.3% polyethylenimine for 30 min) and washed with cold Tris buffer (91 g l⁻¹ Tris base, 25.5 g l⁻¹ MgCl₂·6H₂O and 3.76 g l⁻¹ EDTA) using a Brandel Harvester (Brandel). Filter pieces were punched out and transferred into 1450-401 96-well plates (PerkinElmer). Rotiscint eco plus (Carl Roth) (200 µl) was added, and the plates were sealed with transparent tape (permanent seal for microplates, PerkinElmer), vigorously shaken for at least 3 h and kept in the dark for at least 1 h before the measurement of radioactivity (d.p.m.) with a MicroBeta2 plate counter (PerkinElmer). Specific binding data (d.p.m.) were plotted against the free radioligand nanomolar concentration (obtained by subtracting the amount of bound radioligand (nM) (calculated from the specifically bound radioligand in d.p.m., the specific activity, and the volume per well) from the total radioligand concentration (nM)) and analysed by a two-parameter equation describing hyperbolic binding (SigmaPlot 11.0, Systat Software Inc.) to obtain K_d and receptor density (B_{max}) values. For K_d values < 1 nM, the B_{max} was kept below 1,200 d.p.m. by choosing an appropriate protein concentration. For K_d values > 1 nM, the B_{max} was kept below 3,300 d.p.m.

Competition-binding experiments. Competition-binding experiments were performed according to the procedure for saturation binding with the following modifications: [³H]UR-MK299 was used undiluted and in the case of Y₁R mutants, for which [³H]UR-MK299 exhibited a K_d value > 3 nM, the total volume per well was 100 µl, that is, in the case of total binding, wells were pre-filled with binding buffer (80 µl), and 10 µl of binding buffer containing [³H]UR-MK299 (tenfold concentrated), and the membrane homogenate (10 µl) were added. The following concentrations of [³H]UR-MK299 were used for competition binding with antagonists: 0.2 nM (wild-type Y₁R, T280^{5,52}A, T212^{5,39}A), 0.3 nM (F173^{4,60}W), 1.1 nM (L279^{6,51}A), 5 nM (Q219^{5,46}A), 7 nM (L215^{5,42}G), 10 nM (I124^{3,36}A, F173^{4,60}A). 1 nM [³H]UR-MK299 was used for competition binding with NPY. The incubation time throughout was 90 min. Unspecific binding was determined in the presence of UR-MK299 (100-fold excess to [³H]UR-MK299). Total binding was between 700 and 3,500 d.p.m. Maximum unspecific binding amounted to ≤30% of total binding. Specific binding data (d.p.m.) were plotted against log(concentration of competitor) and analysed by a four-parameter logistic equation (log(inhibitor) versus response-variable slope, GraphPad Prism Software 5.0) to obtain pIC₅₀ values, which were converted to half-maximal inhibitory concentration (IC₅₀) values (pIC₅₀ = -log₁₀(IC₅₀)). In case of incomplete displacement of [³H]UR-MK299 (specifically bound radioligand at the highest competitor concentration between 20% and 50%), pIC₅₀ values were determined by plotting log(B/(B₀ - B)) (Hill plot; B denotes specifically bound radioligand in the presence of competitor (values between 10 and 90%), B₀ is the specifically bound radioligand in the absence of competitor (B₀ = 100%)) against log(competitor concentration) (at least three data points) and pIC₅₀ values (log(B/(B₀ - B)) = 0) were determined by linear regression. K_i values were calculated from the IC₅₀ value as well as the respective K_d value (Extended Data Table 3) and the concentration of [³H]UR-MK299 according to the Cheng-Prusoff equation³⁹.

Inositol phosphate accumulation assay. The signal transduction assay was performed as previously described^{40,41}. In brief, COS-7 cells (obtained from American Type Culture Collection, and species specificity verified by COI DNA barcoding) were seeded into 48-well plates and were transiently co-transfected with wild-type receptor or receptor mutant and a chimeric G protein (G_{αΔ6qj4myr}) plasmid DNA⁴². Cells were routinely tested for mycoplasma contamination. Cells were radioactively labelled with myo[2-³H]inositol (Perkin Elmer) overnight, and then stimulated with an increased concentration of NPY (NPY curve). For antagonist curves, cells were stimulated with the antagonist (BIBP3226: 10⁻⁵ M, BIBO3304: 10⁻⁶ M, MK-HU404: 10⁻⁷ M, UR-MK289: 10⁻⁵ M, UR-MK299: 10⁻⁷ M) parallel to an increased concentration of NPY for 1 h (standard conditions). After cell lysis, anion exchange chromatography was performed and isolated, radioactive accumulated inositol phosphate derivatives were analysed by liquid scintillation counting (scintillation cocktail Optiphas HiSafe, Perkin Elmer).

Using GraphPad Prism 5.0 (GraphPad Software) the determined concentration response curves were analysed. The curves were normalized to the top (100%) and bottom (0%) values of the associated NPY curve. All curves of independent experiments were summarized to one single concentration response curve by the row means total function. Using nonlinear regression (curve fit) the EC₅₀ and pEC₅₀ ± s.e.m. were examined. The shift between the NPY and NPY/antagonist curves is defined as the EC₅₀ ratio and calculated by dividing EC₅₀(NPY/antagonist)/EC₅₀(NPY), the Hill slope was set to 1. All experiments were performed at least two times independently in technical duplicate.

Live-cell fluorescence microscopy. The membrane localization of Y₁R and receptor mutants was verified by fluorescence microscopy. COS-7 cells were seeded in 8-well µ-slides (IBIDI treat) and transiently transfected with Lipofectamine 2000 transfection reagent (Invivogen, Toulouse, France). Twenty-four hours after transfection, nuclei were stained with Hoechst33342 (Sigma-Aldrich) and images were recorded using an ApoTome Imaging System, AxioVert Observer Z1 (YFP: Filter Set 46, DAPI: Filter Set 49, ApoTome, 63×/1.40 oil objective, ZEISS) in a quasi-confocal setting. The data demonstrate that all the mutants are expressed at similar, and wild-type-like, level in COS-7 cells (Extended Data Fig. 2).

Quantification of receptor surface expression in COS-7 cells. COS-7 cells were seeded into black 96-well plates (Greiner), and transiently transfected with a plasmid encoding a receptor-eYFP fusion protein using MetafectenePro. Twenty-four hours after transfection, cells were washed once with HBSS, and fluorescence was quantified using a plate reader (Tecan Infinite M200, Tecan, Männedorf, Switzerland) at excitation 488/5 nm and emission 530/5 nm. Data were normalized to mock transfected (0%) and wild-type Y₁R-eYFP (100%). Results represent mean ± s.e.m. from three independent experiments performed in quadruplicate.

Peptide synthesis. Porcine NPY (YPSKPDNPGEDAPAE DLARYSALRH YINLITRQRY-NH₂) and NPY analogues were synthesized by automated solid-phase peptide synthesis on an automated multiple peptide synthesis robot system (Syro, MultiSynTech), using a 9-fluorenylmethoxycarbonyl-*tert*-butyl (Fmoc/tBu) strategy in 15 µM scale as previously described⁴³. NPY-tyramide was synthesized as previously described⁴⁴. Isotopically labelled NPY variants were prepared as described¹⁶, and ¹³C/¹⁵N-labelled amino acids were coupled manually with 2 equivalents (equiv.) hydroxybenzotriazole/ N,N'-diisopropylcarbodiimide (DIC) in DMF overnight. The porcine variant of NPY, which contains a single mutation M17L was used. This variant has binding affinity and signalling properties that are identical to human NPY and will therefore be referred to as wild-type NPY⁴⁵. It also has increased solubility to assist in handling.

Modified NPY analogues [Bpa¹, K⁴[(Ahx)₂-biotin]]NPY and [K⁴[(Ahx)₂-biotin]]NPY were synthesized by automated solid-phase peptide synthesis and Bpa, Ahx and biotin were coupled manually using orthogonal 1-(4,4-dimethyl-2,6-dioxocyclohexylidene)ethyl (Dde) protection groups, cleaved by freshly prepared 3% (v/v) hydrazine in DMF for 10 × 5 min. Manual coupling reactions were performed by incubation of the resin with 5 equiv. of the respective amino acid, 5 equiv. HOBT and 5 equiv. DIC in DMF for 2 h.

For biotin labelling, 3 equiv. biotin was dissolved in DMF for 10 min at 60 °C. Next, 3 equiv. HOBT and 3 equiv. DIC were added to the mixture. Coupling was performed overnight at room temperature under constant shaking. Bpa containing peptides were cleaved from the resin and completely deprotected with a mixture of trifluoroacetic acid (TFA)/thioanisole (TA)/water (90:5:5 v/v/v).

All peptides were purified by preparative reversed-phase high-performance liquid chromatography (RP-HPLC) on a Jupiter 4 µ Proteo RP-C18 column (90 Å, 4 µm, Phenomenex), Kinetex 5 µ XB-C18 column (100 Å, 5 µm, Phenomenex), Kinetex 5 µ Biphenyl (100 Å, 5 µm, Phenomenex), Aeris 3.6 µm WIDEPORE XB-C18 (200 Å, 3.6 µm, Phenomenex) or Varitide RPC (200 Å, 6 µm, Agilent Technologies). All peptides were characterized by matrix-assisted laser desorption/ionization time of flight (MALDI-TOF) mass spectrometry (Ultraflex III MALDI-TOF/TOF, Bruker daltonics) and ESI-HCT (high-capacity ion trap electrospray-ionization mass spectrometry, Bruker Daltonics). Peptide purities were determined by two different analytical RP-HPLC systems using 0.1% (v/v) TFA in H₂O (eluant A) and 0.08% (v/v) TFA in acetonitrile (ACN) (eluant B). Purity of all peptides was ≥ 95%.

NMR measurements of Y₁R-bound NPY. Fourteen differently isotopically labelled [U-¹³C/¹⁵N]porcine NPY peptides were prepared by standard fluorenylmethoxycarbonyl (Fmoc) solid-phase synthesis as described previously¹⁶. On the basis of the structure of micelle-bound NPY, the positions of the NMR labels were chosen to avoid signal overlap in ¹³C-¹³C single quantum/double quantum correlation experiments and to allow straightforward signal assignment.

Expression of the human Y₁R in *Escherichia coli* as inclusion bodies, inclusion body preparation, solubilization of the receptor in SDS and receptor purification were as described⁴⁶ yielding ~40–50 mg Y₁R per litre of expression medium. To assemble the Y₁R into a functional state, a three-step folding protocol was applied. In step 1, the purified Y₁ receptor was dialysed against a degassed buffer containing 2 mM SDS, 50 mM NaP, pH 8.5, 1 mM EDTA, 1 mM reduced glutathione, and

0.5 mM oxidized glutathione at room temperature for 48 h. Subsequently, 25% (w/w) poly(ethylene glycol) (molecular mass 20 kDa) was added to the buffer to concentrate the receptor before reconstitution. In step 2, bicelles consisting of 1,2-dimyristoyl-*sn*-glycero-3-phosphocholine (DMPC) and 1,2-diheptanoyl-*sn*-glycero-3-phosphocholine (DHPC-C7) (AvantiPolarLipids) with a q value of 0.25 in 50 mM NaP, pH 8.0 were incubated with Y₁R, with three subsequent cycles of fast temperature cycles from 42 °C to 0 °C. Aggregated protein was removed instantly by centrifugation. In step 3, the Y₁R samples were concentrated in large bicelles ($q > 20$), which were used instead of liposomes because of the high achievable receptor packing⁴⁶. In large bicelles, all receptor binding sites are fully accessible. Subsequently, 50 mg ml⁻¹ BioBeadsSM2 was added at least twice to the solution. After removal of the beads with a sieve, samples were washed four times through cycles of pelleting by centrifugation and resolubilization in 50 mM NaP, pH 7.0. Concentration determination of the membrane embedded receptor was performed by solubilization of the bicelles in ten times the volume of 15 mM SDS and 50 mM NaP, pH 7.0 and subsequent measurement of the Y₁R intrinsic absorption at 280 nm using UV-visible spectroscopy. Labelled NPY variants in a slight molar excess were added to the Y₁R after detergent removal but before concentrating.

Assessment of the binding affinity of the Y₁R was carried out using homogenous fluorescence assays as described in the literature⁴⁷. The reconstituted receptor was incubated in increasing concentrations with 50 nM fluorescently labelled NPY (NPY-atto520) overnight at room temperature in 50 mM NaP, pH 7.0 and 0.1% BSA. The fluorescence spectra were recorded on a FluoroMax-2 (JOBIN YVON) in a 10 mm quartz cuvette at 20 °C. The maximum signals of each spectrum were determined, normalized and plotted against the receptor concentration. The inflection point for Y₁R binding was determined (OriginPro 8 G / DoseResp) at EC₅₀ = 52 nM, demonstrating high functionality of the system. As a control, we used empty bicelles in concentrations that matched the bicelle concentration of the receptor samples, resulting in a lower binding ability to the ligand in comparison to the Y₁R.

NMR spectra were recorded on a Bruker Avance III 600 NMR spectrometer. The ¹³C cross-polarization magic angle spinning (MAS) NMR experiments (0.7 ms contact time) were carried out using a double-resonance MAS probe with a 4 mm spinning module. Typical 90° pulse lengths were 4 μs for ¹H and ¹³C and heteronuclear decoupling (SPINAL64) at a field strength of ~65 kHz. The ¹³C chemical shifts were referenced relative to tetramethylsilane. The experiments were conducted at -30 °C and an MAS frequency of 7 kHz. The ¹³C double quantum ¹³C single quantum correlation spectra were acquired using the SPC-5 recoupling sequence⁴⁸ for double quantum excitation and reconversion (set to 0.571 ms each). The relaxation delay was 2.4 s.

Molecular docking of NPY into Y₁R. Peptide docking of full-length porcine NPY was completed using Rosetta's FlexPepDock application⁴⁹. In brief, low energy backbone conformations were generated from the starting conformation of UR-MK299-bound Y₁R. Initially, the trimer of C-terminal NPY was docked into these conformations using full flexible docking guided by mutagenesis data. For each round of docking 5,000 models were generated. The models were sorted by total energy and binding energy. Top models from a given docking round were used to seed the next round of docking in which the peptide was extended. Fragment picking was performed using the fragment_picker application within Rosetta²⁶. Secondary structure during fragment picking was guided by the NMR chemical shift data. Additionally, experimentally derived restraints were used to guide docking (R35-D287^{6,59}, R35-N283^{6,55}, Y36-Y100^{2,64}, R33-N299^{7,32}, L30-I293^{HEL33}). After docking peptides of length 6, 12, 18 and 36, the binding pocket was resampled to allow the ligand binding pocket to adapt to the shape of the peptide. This was accomplished with RosettaCM⁵⁰. The Y₁R crystal structure was used as a template along with the docked model to ensure the models did not drift too far from the starting structure though the N terminus was removed until the last docking step to provide steric bulk. Following full-length NPY docking, the N terminus of NPY was localized using loose distance constraints with the peptides identified in crosslinking experiments. Model selection from RosettaCM was accomplished using clustering to ensure backbone diversity. Following the identification of docked poses that satisfied the majority of experimental data, the chemical shifts of docked NPY peptides were calculated and filtered against the experimental NMR data to generate a final ensemble of docked poses with a 1.4 p.p.m. root mean square distance to the experimental data. To analyse the binding interactions, per residue energetic analysis was calculated using the residue_energy_breakdown algorithm. The model with the lowest energy was selected as the representative binding pose (Fig. 4a). The ensemble is rather tight and therefore the individual binding poses are similar in overall structure (Fig. 4b).

Photo-crosslinking experiment between Y₁R and NPY N terminus. Cell-free expressed Y₁R was produced by coupled in vitro transcription-translation performed as previously described⁵¹ using a bacterial cell lysate (S30 extract) from *E. coli* BL21 (DE3). Soluble membrane protein expression was achieved by

addition of 0.1% (w/v) Brij-58, 1 mM oxidized glutathione (GSSG) and 5 mM reduced glutathione (GSH). Expression buffer was then exchanged to a binding buffer (0.1 M Tris/HCl, pH 7.4, 5% glycerol and 0.1% (w/v) Brij-58) and samples were purified by ligand affinity chromatography using [K⁴[(Ahx)₂-biotin]]NPY immobilized on Pierce Avidin Agarose beads (Thermo Fisher Scientific) as previously described⁵². Elution was performed using 60 mM CaCl₂.

For photo-crosslinking Y₁R in binding buffer was incubated with [Bpa¹, K⁴[(Ahx)₂-biotin]]NPY in a molar ratio of 4:1 (5 nmol:1.25 nmol) for 30 min at room temperature. In addition, the same reaction was performed with an eightfold-excess of NPY (Y₁R:[Bpa¹, K⁴[(Ahx)₂-biotin]]NPY:NPY, 4:1:8). Subsequently, the opened reaction vessels were placed on ice and irradiated with UV light (UV lamp, Atkas Fluorescent forte, λ = 366 nm, 180 W) for 90 min. 50 μl of photo-crosslinked Y₁R sample (~200 μg) was digested with Glu-C and rLys-C (Promega) according to the manufacturer's protocol. Crosslinked fragments were then isolated by affinity purification using Monomeric Avidin Agarose beads (Thermo Fisher Scientific) according to the manufacturer's protocol. Possible fragments of digested Y₁R were calculated using the online tool PeptideMass⁵³. To account for incomplete digestion the tool allowed for a maximum of five missed cleavages. For the analysis the combined option 'Glu C (phosphate) + Lys-C' was chosen. The same procedure was used for the calculation of possible NPY fragments. Theoretical masses of fragments after enzymatic cleavage of photo-crosslinked Y₁R-[Bpa¹, K⁴[(Ahx)₂-biotin]]NPY were calculated by adding possible Y₁R fragment masses to NPY fragment masses containing the N terminus. The masses of Bpa, two times Ahx and biotin reduced by water were added manually to account for the formation of a peptide bond. Peptide fragments of photo-crosslinked Y₁R were analysed by MALDI-TOF mass spectrometry using an Ultraflex III MALDI-TOF/TOF mass spectrometer (Bruker Daltonics).

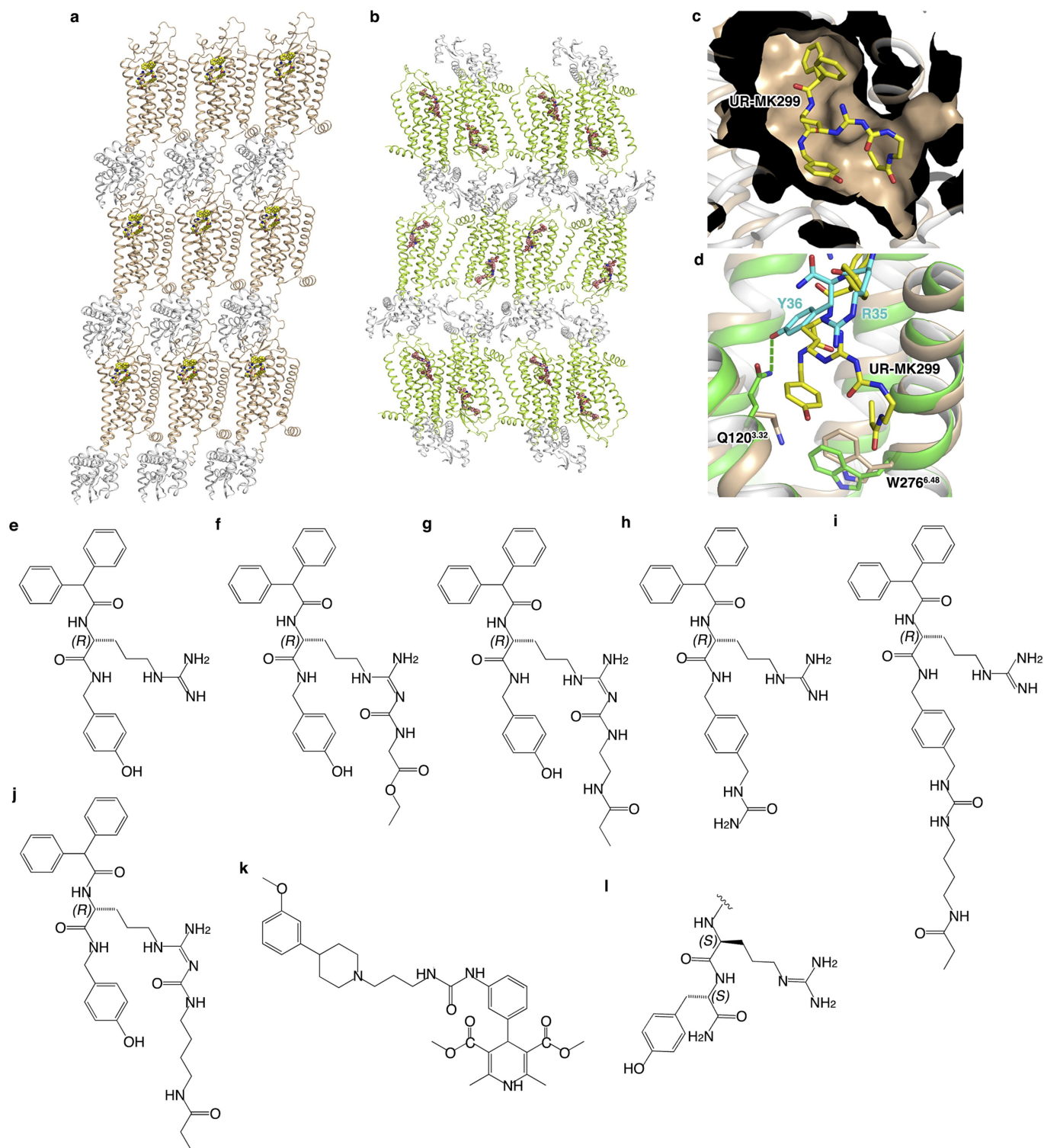
Functionality of cell-free expressed Y₁R samples was verified by a homogenous binding assay based on fluorescence polarization. We used [Dpr22-Atto 520]NPY (hereafter: NPY-Atto 520) as a fluorescence tracer (inositol phosphate accumulation in transiently transfected COS-7: EC₅₀ = 24 nM, pEC₅₀ = -7.61 ± 0.20). 50 nM of NPY-Atto 520 was incubated with increasing concentrations of Y₁R in Brij-58 micelles in buffer (0.1 M Tris/HCl, pH 7.4, 2.5% glycerol, 0.1% (w/v) Brij-58 and 0.1% bovine serum albumin) for 90 min under gentle agitation in opaque 96-well plates. Fluorescence was then measured in a Tecan Spark plate reader (Tecan) using linear polarized light (excitation 510/5 nm, emission 550/10 nm, 90° detection angle). Experiments were conducted at least twice independently in duplicate.

Reporting summary. Further information on experimental design is available in the Nature Research Reporting Summary linked to this paper.

Data availability. Atomic coordinates and structure factor files for the Y₁R-UR-MK299 and Y₁R-BMS-193885 complex structures have been deposited in the Protein Data Bank (PDB) with accession codes 5ZBQ and 5ZBH, respectively.

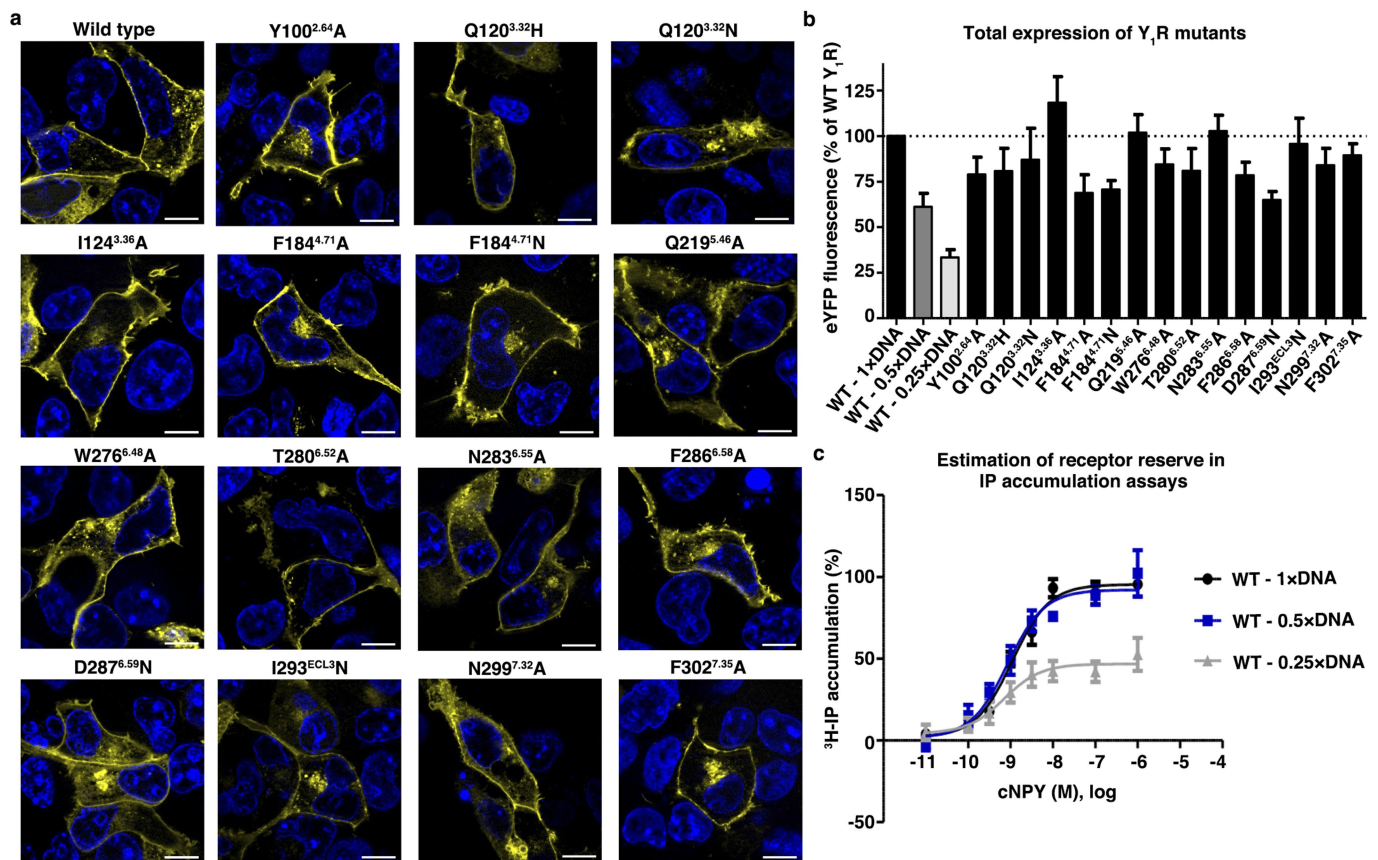
- Rosenbaum, D. M. et al. GPCR engineering yields high-resolution structural insights into β₂-adrenergic receptor function. *Science* **318**, 1266–1273 (2007).
- Roth, C. B., Hanson, M. A. & Stevens, R. C. Stabilization of the human β₂-adrenergic receptor TM4–TM5 helix interface by mutagenesis of Glu122^{3,41}, a critical residue in GPCR structure. *J. Mol. Biol.* **376**, 1305–1319 (2008).
- Kabsch, W. XDS. *Acta Crystallogr. D* **66**, 125–132 (2010).
- McCoy, A. J. et al. Phaser crystallographic software. *J. Appl. Crystallogr.* **40**, 658–674 (2007).
- Murshudov, G. N. et al. REFMAC5 for the refinement of macromolecular crystal structures. *Acta Crystallogr. D* **67**, 355–367 (2011).
- Smart, O. S. et al. Exploiting structure similarity in refinement: automated NCS and target-structure restraints in BUSTER. *Acta Crystallogr. D* **68**, 368–380 (2012).
- Emsley, P., Lohkamp, B., Scott, W. G. & Cowtan, K. Features and development of Coot. *Acta Crystallogr. D* **66**, 486–501 (2010).
- Keller, M. et al. Mimicking of arginine by functionalized N^ε-carbamoylated arginine as a new broadly applicable approach to labeled bioactive peptides: high affinity angiotensin, neuropeptide Y, neuropeptide FF, and neurotensin receptor ligands as examples. *J. Med. Chem.* **59**, 1925–1945 (2016).
- Yung-Chi, C. & Prusoff, W. H. Relationship between the inhibition constant (K_i) and the concentration of inhibitor which causes 50 per cent inhibition (I₅₀) of an enzymatic reaction. *Biochem. Pharmacol.* **22**, 3099–3108 (1973).
- Burkert, K. et al. A deep hydrophobic binding cavity is the main interaction for different Y₂R antagonists. *ChemMedChem* **12**, 75–85 (2017).
- Els, S., Beck-Sickinger, A. G. & Chollet, C. Ghrelin receptor: high constitutive activity and methods for developing inverse agonists. *Methods Enzymol.* **485**, 103–121 (2010).
- Kostenis, E. Is Gα₁₆ the optimal tool for fishing ligands of orphan G-protein-coupled receptors? *Trends Pharmacol. Sci.* **22**, 560–564 (2001).
- Pedragosa-Badia, X. et al. Pancreatic polypeptide is recognized by two hydrophobic domains of the human Y₄ receptor binding pocket. *J. Biol. Chem.* **289**, 5846–5859 (2014).
- Hoffmann, S., Rist, B., Videnov, G., Jung, G. & Beck-Sickinger, A. G. Structure-affinity studies of C-terminally modified analogs of neuropeptide Y led to a novel class of peptidic Y₁ receptor antagonist. *Regul. Pept.* **65**, 61–70 (1996).

45. Gerald, C. et al. A receptor subtype involved in neuropeptide-Y-induced food intake. *Nature* **382**, 168–171 (1996).
46. Schmidt, P. et al. A reconstitution protocol for the in vitro folded human G protein-coupled Y₂ receptor into lipid environment. *Biophys. Chem.* **150**, 29–36 (2010).
47. Casiraghi, M. et al. Functional modulation of a G protein-coupled receptor conformational landscape in a lipid bilayer. *J. Am. Chem. Soc.* **138**, 11170–11175 (2016).
48. Hohwy, M., Rienstra, C. M., Jaroniec, C. P. & Griffin, R. G. Fivefold symmetric homonuclear dipolar recoupling in rotating solids: application to double quantum spectroscopy. *J. Chem. Phys.* **110**, 7983–7992 (1999).
49. Raveh, B., London, N., Zimmerman, L. & Schueler-Furman, O. Rosetta FlexPepDock ab-initio: simultaneous folding, docking and refinement of peptides onto their receptors. *PLoS ONE* **6**, e18934 (2011).
50. Song, Y. et al. High-resolution comparative modeling with RosettaCM. *Structure* **21**, 1735–1742 (2013).
51. Schwarz, D. et al. Preparative scale expression of membrane proteins in *Escherichia coli*-based continuous exchange cell-free systems. *Nat. Protocols* **2**, 2945–2957 (2007).
52. Bosse, M. et al. Assessment of a fully active class A G protein-coupled receptor isolated from in vitro folding. *Biochemistry* **50**, 9817–9825 (2011).
53. Wilkins, M. R. et al. Detailed peptide characterization using PEPTIDEMASS—a World-Wide-Web-accessible tool. *Electrophoresis* **18**, 403–408 (1997).



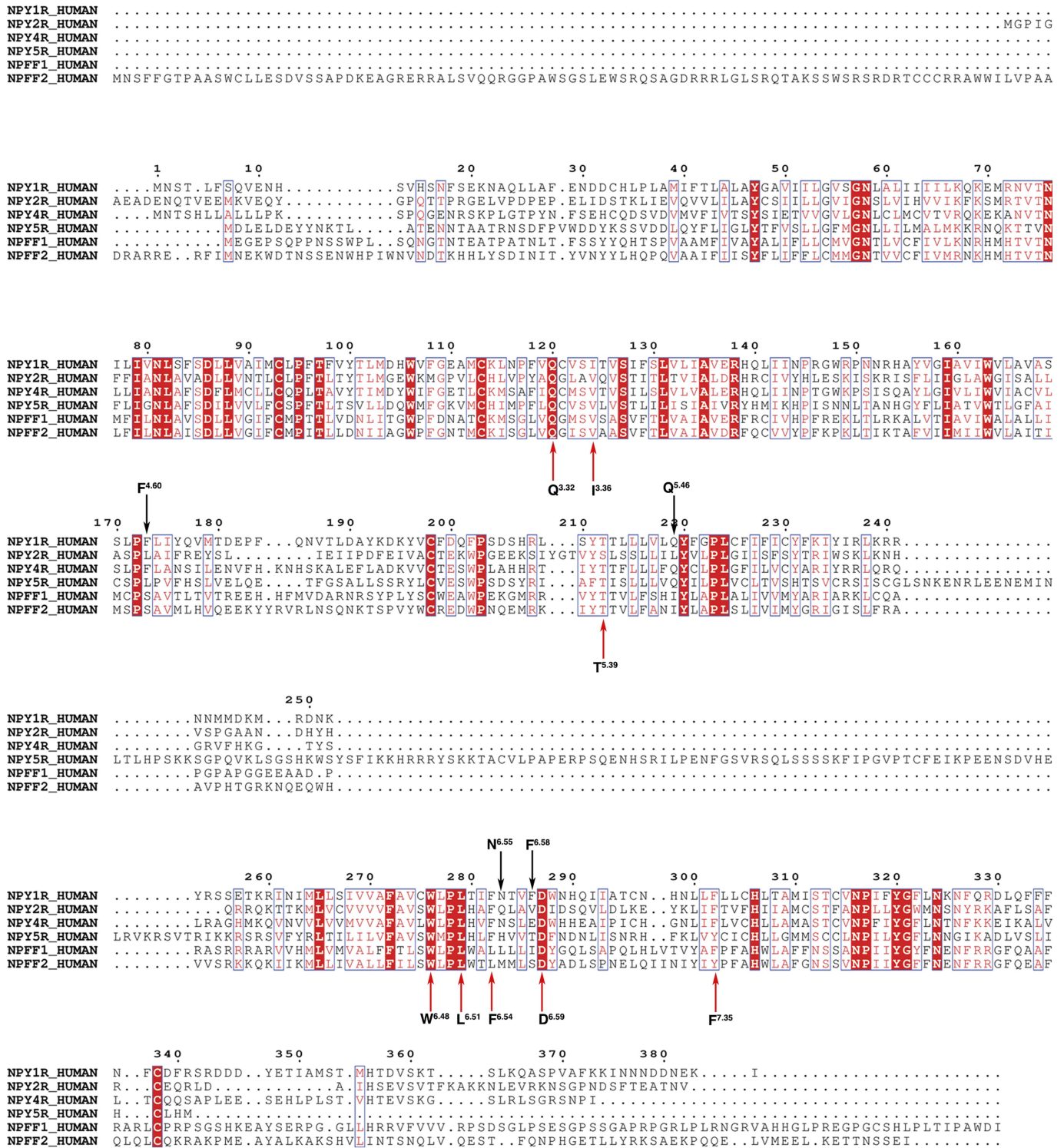
Extended Data Fig. 1 | Crystal packing and structural features of Y_1R and chemical structures of Y_1R ligands. **a, b,** Crystal packing of Y_1R -UR-MK299 (**a**) and Y_1R -BMS-193885 (**b**) complexes. Y_1R is shown in cartoon representation and coloured brown and green in the Y_1R -UR-MK299 and Y_1R -BMS-193885 complexes, respectively. The T4L fusion is shown in grey cartoon representation. UR-MK299 and BMS-193885 are displayed as yellow and pink spheres, respectively. **c,** Cutaway view of the UR-MK299-binding pocket in Y_1R . The receptor is shown in brown cartoon and surface representations. The ligand is shown as yellow sticks. **d,** Comparison of Y_1R in the Y_1R -UR-MK299 crystal structure (brown)

and the Y_1R -NPY model (green). Side chains of Q120^{3,32} and W276^{6,48} are shown as sticks. R35-Y36 of NPY is displayed as cyan sticks. The hydrogen bond between Q120^{3,32} and Y36 of NPY is shown as a green dashed line. **e-j,** Chemical structures of the arginamide Y_1R antagonists BIBP3226 (**e**), UR-HU404 (**f**), UR-MK299 (**g**), BIBO3304 (**h**), UR-MK289 (**i**) and UR-MK136 (**j**). **k,** Chemical structure of BMS-193885. **l,** Scaffold of NPY C-terminal residues R35 and Y36. Key differences between R35-Y36 of NPY and UR-MK299 are chirality of the arginine derivative and alteration of bond connectivity leading to the hydroxyphenyl group.



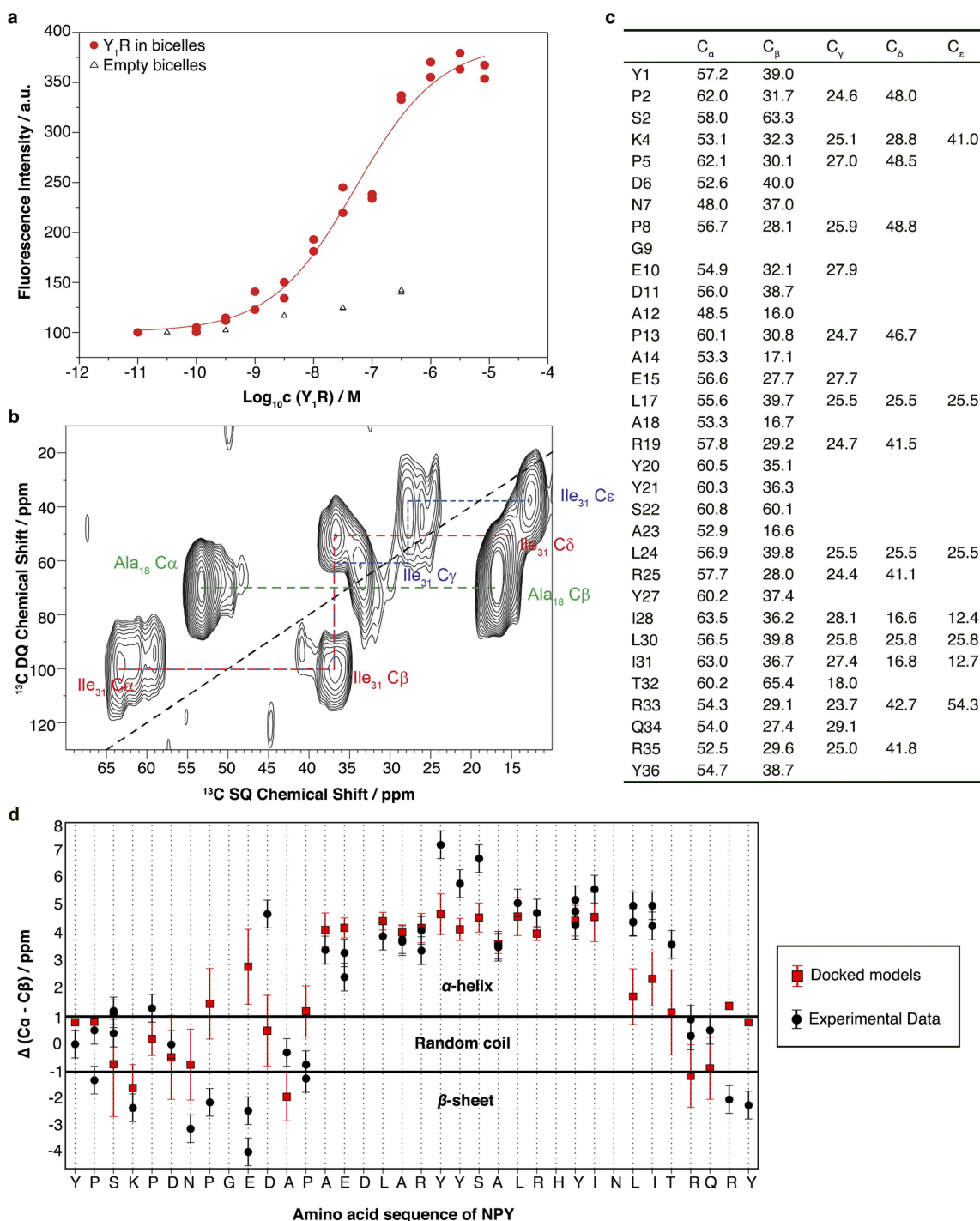
Extended Data Fig. 2 | Expression of wild-type and mutant Y_1 receptors in transiently transfected COS-7 cells. **a**, Live-cell fluorescence microscopy verifies all Y_1R variants to be properly folded and exported to the cell membrane like the wild-type receptor. Nuclei stained with Hoechst33342. Scale bars, 10 μ m. Pictures are representative of two independent experiments with similar results. **b**, The total expression level was determined by fluorescence reading and expression was confirmed to be similar to the wild type. Transfection of only 50% or 25% of the DNA amount (with total DNA amount held constant by empty vector), led to a proportional decrease of fluorescence, and thus, expression level. Data represent mean \pm s.e.m. of three to five independent experiments

performed in technical triplicate (see Source Data for sample size of each mutant). **c**, Estimation of the receptor reserve in functional inositol phosphate accumulation assays. Transfection of half of the vector encoding the receptor (with a constant total DNA amount including chimeric G protein, see **a**) still produces maximum signal, while further reduction results in signal loss at comparable potency. Thus, there is only a small receptor reserve in the functional readout, allowing potency alteration to be directly related to compromised ligand binding. Data represent mean \pm s.e.m. of three independent experiments performed in technical duplicate. cNPY, concentration of NPY.



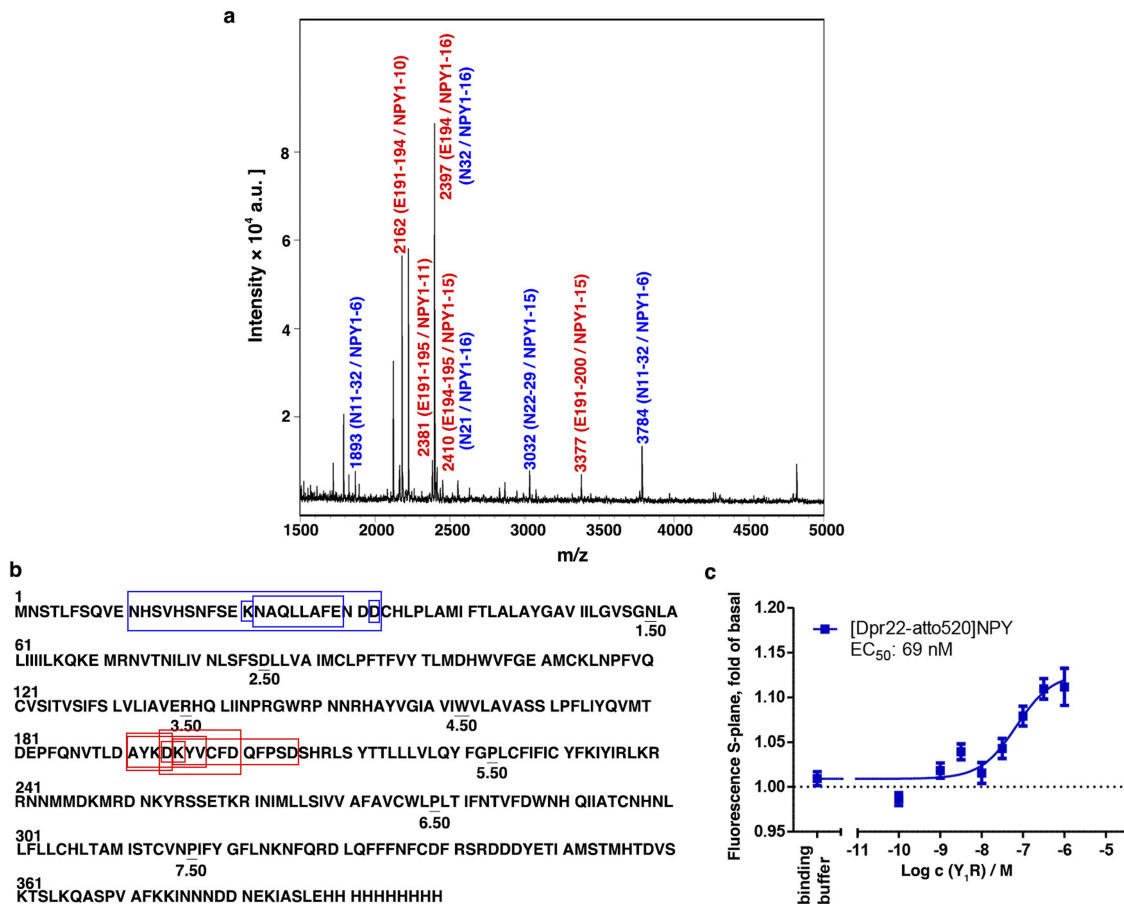
Extended Data Fig. 3 | Sequence alignment of the human NPY receptors and the human NPPF receptors. Colours represent the similarity of residues: red background, identical; red text, strongly similar. Key residues in the UR-MK299-binding pocket, which are conserved or variable among

receptors, are indicated by red or black arrows, respectively. The alignment was generated using UniProt (<http://www.uniprot.org/align/>) and the graphic was prepared on the ESPrpt 3.0 server (<http://esprpt.ibcp.fr/ESPrpt/cgi-bin/ESPrpt.cgi>).



Extended Data Fig. 4 | Pharmacological characterization of refolded Y_1R and NMR studies of Y_1R -bound NPY. **a**, Binding of Atto 520-labelled NPY (50 nM) to increasing amounts of bicelles containing Y_1R or empty bicelles. Data reflect fluorescence enhancement upon binding. An inflection point at $EC_{50} = 52$ nM was determined. Two independent experiments were performed in technical duplicate with similar results. Data shown are from a representative experiment. a.u., arbitrary units. $c(Y_1R)$, concentration of Y_1R . **b**, Typical ^{13}C MAS single-quantum (SQ)/double-quantum (DQ) correlation spectrum of NPY in the presence of Y_1R reconstituted into large bicelles at $-30^\circ C$. NMR spectra were acquired from one to three independent preparations for each labelled amino acid with similar results (see **d**). Data shown are from a representative experiment. **c**, Table showing ^{13}C -NMR chemical

shifts of assigned amino acids of NPY bound to Y_1R (referenced to tetramethylsilane) as acquired in solid-state NMR experiments. **d**, ^{13}C -chemical-shift index of NPY bound to Y_1R in large DMPC/DHPC-c7 bicelles ($q > 20$) compared with docked models. Plotted in black is the measured chemical shift difference ($C_\alpha - C_\beta$) for each individual residue of NPY minus the chemical shift difference of the same amino acid type in random-coil conformation. Individual data points from one to three independent experiments for each labelled amino acid are shown. Typical experimental error when determining chemical shifts under these conditions are ± 1 p.p.m. Chemical shifts were back-calculated for the top docking solutions and filtered against the experimental data to generate a final ensemble of docked poses. Their average chemical-shift index and associated s.d. from the top ten docked poses are shown in red.



Extended Data Fig. 5 | Photo-crosslinking experiments between NPY and Y₁R. **a**, Mass spectra of photo-crosslinked Y₁R with [Bpa¹, K⁴[(Ahx)₂-biotin]]NPY. Exemplary MALDI-TOF mass spectra of photo-crosslinked samples enzymatically digested by rLys-C and Glu-C. Potential Y₁R fragments are labelled. Two independent experiments were performed with similar results. N, N terminus of Y₁R (blue); E, ECL2 (red). **b**, Respective regions of NPY N terminus at Y₁R. Amino acid sequence of Y₁R with a C-terminal His-tag. The two detected regions within Y₁R (N terminus (blue), ECL2 (red)) after crosslinking with [Bpa¹, K⁴[(Ahx)₂-biotin]]NPY are emphasized in boxes. The different sizes of the boxes

represent different detected fragments (Extended Data Table 5). Experiments were repeated twice independently with similar results, and only fragments that were observed in both experiments are listed here and in Extended Data Table 5. **c**, Binding of Atto 520-labelled NPY (50 nM) to increasing amounts of cell-free produced Y₁R in Brij-58. Data reflect fluorescence enhancement upon binding. An EC₅₀ value of 69 nM was determined. Data shown are mean ± s.e.m. from six independent experiments performed in technical triplicate. c(Y₁R), concentration of Y₁R.

Extended Data Table 1 | Data collection and refinement statistics

	Y ₁ R-UR-MK299	Y ₁ R-BMS-193885
Data Collection*		
Space group	<i>P</i> 2 ₁	<i>C</i> 222 ₁
Cell dimensions		
<i>a</i> , <i>b</i> , <i>c</i> (Å)	37.8, 100.7, 83.2	76.9, 126.8, 170.3
α, β, γ (°)	90.0, 98.8, 90.0	90.0, 90.0, 90.0
Resolution (Å)	50.0-2.70 (2.83-2.70) [†]	50.0-3.0 (3.1-3.0)
<i>R</i> _{merge} (%)	17.0 (86.1)	16.6 (93.7)
<i>I</i> / <i>σ</i> <i>I</i>	4.78 (0.97)	5.30 (1.00)
Completeness (%)	97.3 (96.9)	92.4 (79.2)
Redundancy	4.0 (3.6)	3.5 (2.6)
Refinement		
Resolution (Å)	50.0-2.7	50.0-3.0
No. reflections	16,520 (790)	15,600 (797)
<i>R</i> _{work} / <i>R</i> _{free} (%)	22.5 / 24.7	22.4 / 24.9
Number of atoms		
Protein	3,715	3,654
Ligand	45	43
Overall <i>B</i> values (Å ²)		
Protein	88.2	108.0
Ligand	65.2	81.0
R.m.s. deviations		
Bond lengths (Å)	0.010	0.009
Bond angles (°)	1.04	1.00

*Diffraction data from 47 Y₁R-UR-MK299 crystals and 33 Y₁R-BMS-193885 crystals were used to solve the structures.

[†]Numbers in parentheses refer to the highest-resolution shell.

Extended Data Table 2 | Inositol phosphate accumulation assays of wild-type and mutant Y₁ receptors for NPY and antagonists

Mutants	NPY					NPY/BIBP3226 (10 ⁻⁵ M)*					NPY/BIBO3304 (10 ⁻⁶ M)					NPY/UR-HU404 (10 ⁻⁷ M)					NPY/UR-MK289 (10 ⁻⁵ M)					NPY/UR-MK299 (10 ⁻⁷ M)				
	EC ₅₀ (nM) [†] (pEC ₅₀ ± SEM)	n [‡]	EC ₅₀ (nM) (pEC ₅₀ ± SEM)	Ratio [§]	K _b (nM)	n	EC ₅₀ (nM) (pEC ₅₀ ± SEM)	Ratio	K _b (nM)	n	EC ₅₀ (nM) (pEC ₅₀ ± SEM)	Ratio	K _b (nM)	n	EC ₅₀ (nM) (pEC ₅₀ ± SEM)	Ratio	K _b (nM)	n	EC ₅₀ (nM) (pEC ₅₀ ± SEM)	Ratio	K _b (nM)	n								
Wild type	1.7 (8.78 ± 0.03)	20	463 (6.43 ± 0.04)	272	36.9	14	175 (6.76 ± 0.04)	103	9.8	16	1,099/126 [#] (5.96 ± 0.04)/ (6.90 ± 0.07)	646/ 74 [#]	0.16/ 0.14 [#]	14	228 (6.64 ± 0.04)	134	75.2	15	250 (6.60 ± 0.06)	147	0.69	10								
Y100 ⁶⁴ A	562; 404	2	nd	nd	nd	2	nd	nd	nd	2	nd	nd	nd	2	nd	nd	nd	2	/	/	/	/								
Q120 ³³² H	12; 15	2	nd	nd	nd	2	nd	nd	nd	2	>50,000; >50,000	>3,500	<0.03	2	>50,000 >50,000	>3,500	<2.86	2	>50,000 >50,000	>3,500	<0.03	2								
Q120 ³³² N	3.8 (8.42 ± 0.07)	4	836 (6.08 ± 0.06)	220	45.7	3	414 (6.38 ± 0.09)	109	9.3	3	3,744 (5.43 ± 0.10)	985	0.10	3	325 (6.49 ± 0.08)	86	118	3	743 (6.13 ± 0.06)	196	0.51	3								
I124 ³³⁶ A	6.0 (8.22 ± 0.08)	3	1,877 (5.73 ± 0.06)	313	32.1	4	306 (6.52 ± 0.06)	51	20.0	4	1,588 (5.80 ± 0.06)	265	0.38	4	637 (6.20 ± 0.08)	106	95.2	4	208 (6.68 ± 0.09)	35	2.94	4								
Q219 ⁶⁴⁶ A	23 (7.63 ± 0.05)	7	2,732 (5.56 ± 0.08)	119	84.8	4	1,156 (5.94 ± 0.07)	50	20.4	3	>10,000/ 1,711 [#] / 2,197 [#]	>435/ 74 [#] / 96 [#]	<0.23/ 0.14 [#] / 0.11 [#]	3/2 [#]	5,518 (5.26 ± 0.12)	240	41.8	3	1146; 793 50; 34	2.05; 3.0	2									
W276 ⁶⁴⁸ A	3.8 (8.42 ± 0.06)	5	246 (6.61 ± 0.12)	65	156	3	84; 60	22; 16	47; 68	2	490; 254	129; 67	0.8; 1.5	2	1,445; 1505 380; 396	26; 25	2	140; 87 37; 23	2.8; 4.6	2										
T280 ⁶⁵² A	2.6 (8.58 ± 0.08)	4	141 (6.85 ± 0.08)	54	189	4	124 (6.91 ± 0.05)	48	21.3	4	871 (6.06 ± 0.08)	335	0.30	4	278 (6.56 ± 0.07)	107	94.3	3	306 (6.51 ± 0.06)	118	0.86	3								
N283 ⁶⁵⁵ A	900 (6.05 ± 0.06)	7	1,148 (5.94 ± 0.12)	1	nd	3	1,036 (5.98 ± 0.14)	1	nd	3	7,622 (5.12 ± 0.14)	8	14.3	3	1,193 (5.92 ± 0.14)	1	nd	3	495; 571	1	nd	2								
F286 ⁶⁵⁸ A	4.5 (8.35 ± 0.04)	7	491 (6.31 ± 0.05)	109	92.6	3	118 (6.93 ± 0.09)	26	40.0	3	1,553 (5.81 ± 0.05)	345	0.29	3	126 (6.90 ± 0.07)	28	370	3	180 (6.74 ± 0.16)	40	2.56	3								
D287 ⁶⁵⁹ N	260 (6.59 ± 0.05)	7	900; 748	3.5; 2.9	4065; 5328	2	341; 142	1	nd	2	>20,000; 1,571 [#] / (5.80 ± 0.12)	>77/ 6 [#]	<1.3/ 2.0 [#]	2/3 [#]	729; 504	2.8; 1.9	5,543; 10,655	2	193; 177	1	nd	2								
F302 ⁷³⁵ A	4.2 (8.38 ± 0.09)	3	16; 29	4; 7	3,570; 1,695	2	4.4; 10.1	1; 2.4	nd; 712	2	33; 42	8; 10	14.6; 11.1	2	3.8; 5.2	1	nd	2	9.4 (8.03 ± 0.11)	2	100	3								

nd, not determined; /, not tested.

*Antagonist concentrations were chosen based on their antagonistic activity on Y₁R.

†EC₅₀ values were determined after 1 h stimulation by increasing the concentration of NPY or NPY together with different antagonists. Data are shown as mean values from at least three independent experiments or the results of two individual experiments each performed in technical duplicate.

‡Sample size; the number of independent experiments performed in technical duplicate.

§The EC₅₀ ratio represents the shift between the NPY and NPY + antagonist curve (EC₅₀(NPY + antagonist)/EC₅₀(NPY)) and characterizes the antagonistic effect on the wild-type receptor or receptor mutants. By comparison of EC₅₀ ratios between wild-type and mutant receptor, influences of all tested residues on antagonist activity were determined. A higher ratio indicates higher antagonist activity.

A reduced EC₅₀ ratio of mutant compared to the wild-type receptor was interpreted as important for the respective antagonist.

|| K_b values were determined using the Gaddum transformation (K_b = [antagonist]/(EC₅₀ ratio - 1)).

#These data were obtained at a reduced concentration of UR-HU404 (10⁻⁸ M) as concentration response curves did not reach saturation (EC₅₀ > 10,000 nM) when a higher concentration was used (10⁻⁷ M).

Extended Data Table 3 | Binding of Y₁R antagonists and agonists to membrane preparations from Sf9 cells expressing wild-type and mutant Y₁ receptors

Y ₁ R mutants	K _d (nM)*		K _i (nM) [†]									
	[³ H]-UR-MK299	n [‡]	BMS-193885		BIBP3226		BIBO3304		UR-MK136		UR-MK289	
			n	n	n	n	n	n	n	n		
Wild type	0.17 ± 0.03	3	22 ± 6	3	2.4; 3.1	2	1.6 ± 0.3	3	2.8; 4.0	2	25; 28	2
Crystallization construct	0.33 ± 0.06	3	38 ± 2	4	/		/		/		/	
C121 ^{3,33} A	1.4; 2.4	2	/		/		/		/		/	
I124 ^{3,36} A	7.0; 8.0	2	9,500 ± 1,700	3	15 ± 5	3	11 ± 2	3	12 ± 2	3	80 ± 16	3
I124 ^{3,36} F	1.3; 1.9	2	/		/		/		/		/	
F173 ^{3,60} A	9.1 ± 2.2	4	590 ± 220	3	68; 84	2	120 ± 17	4	88; 110	2	660 ± 110 [§]	5
F173 ^{3,60} W	0.31; 0.32	2	110; 130	2	15; 26	2	13 ± 4	3	3.6; 4.3	2	6.8; 9.2	2
T212 ^{5,39} A	0.12; 0.18	2	150; 150	2	13; 12	2	2.5 ± 0.3	3	5.7; 7.5	2	18; 21	2
L215 ^{5,42} G	4.2; 5.6	2	9.6 ± 1.9	4	43; 23	2	47 ± 4	3	11; 8.4	2	29; 30	2
Q219 ^{5,46} A	4.1; 5.1	2	0.50 ± 0.07	4	35; 53	2	6.2 ± 0.7	3	16 ± 4	3	13 ± 4	3
Q219 ^{5,46} V	5.1 ± 1.2	3	/		/		/		/		/	
W276 ^{6,48} A	>500	3	/		/		/		/		/	
L279 ^{6,51} A	1.0; 1.1	2	160; 220	2	110; 110	2	13 ± 2	3	120; 150	2	320 ± 40	3
T280 ^{6,52} A	0.16 ± 0.04	3	7,300 ± 1,300	3	32 ± 7	3	2.6 ± 0.4	3	4.2 ± 1.1	3	8.2 ± 4.2	3
N283 ^{6,55} A	>500; >500	2	/		/		/		/		/	
D287 ^{6,59} A	>500; >500	2	/		/		/		/		/	
F302 ^{7,35} A	>500; >500	2	/		/		/		/		/	

b. Binding of NPYs to wild-type Y₁R

Y ₁ R	K _d (nM)*		K _i (nM) [†]			
	[³ H]-UR-MK299	n	Human NPY		Porcine NPY	
				n		n
Wild type	0.89; 1.1	2	4.1; 4.2	2	2.8 ± 0.4	4

*Dissociation constant determined by saturation binding at Sf9 membranes (receptor expression was confirmed by western blot analysis) using a sodium-containing buffer (a) or a sodium-free buffer (b) (the sodium-free buffer was used for the determination of agonist binding affinity because porcine NPY exhibited approximately tenfold higher affinity in the sodium-free buffer compared to the sodium-containing buffer (data not shown)).

†Dissociation constant determined by competition binding with [³H]UR-MK299 at Sf9 membranes using a sodium-containing buffer (a) or a sodium-free buffer (b).

‡Sample size; the number of independent experiments performed in technical triplicate. If $n > 2$, data are shown as mean ± s.e.m. If $n = 2$, results of two individual experiments are shown.

§The lower curve plateau of the four-parameter logistic fit, amounting to 17 ± 3% of specifically bound [³H]UR-MK299 (mean ± s.e.m. from five independent experiments), was significantly different from zero ($P < 0.005$, one-sample one-tailed t -test), which is indicative of a non-competitive mechanism.

Extended Data Table 4 | Inositol phosphate accumulation assays of wild-type and mutant Y₁ receptors for NPY and NPY analogues

a. IP accumulation assays of complementary mutagenesis between NPY/NPY analogues and WT and mutant Y ₁ Rs																			
Peptides*	WT			Q120 ^{3,32} H			I293 ^{ECL2} N			N299 ^{7,32} A			N283 ^{6,55} A			D287 ^{6,59} A			
	EC ₅₀ (nM) [†] (pEC ₅₀ ± SEM)	X-fold over WT [‡]	n [§]	EC ₅₀ (nM) (pEC ₅₀ ± SEM)	X-fold over WT	n	EC ₅₀ (nM) (pEC ₅₀ ± SEM)	X-fold over WT	n	EC ₅₀ (nM) (pEC ₅₀ ± SEM)	X-fold over WT	n	EC ₅₀ (nM) (pEC ₅₀ ± SEM)	X-fold over WT	n	EC ₅₀ (nM) (pEC ₅₀ ± SEM)	X-fold over WT	n	
NPY	1.5 (8.83 ± 0.02)	1	51	39 (7.41 ± 0.11)	26	3	169 (6.77 ± 0.08)	113	8	91 (7.04 ± 0.09)	61	5	1,053 (5.98 ± 0.13)	702	6	1,384 (5.86 ± 0.09)	461	3	
[N30]NPY	289 (6.54 ± 0.06)	1	9	/	/	/	3116; 1274	11; 4	2	/	/	/	/	/	/	/	/	/	/
[A33]NPY	5,395 (5.27 ± 0.07)	1	3	/	/	/	/	/	/	5,306 (5.28 ± 0.07)	1	3	/	/	/	/	/	/	/
[A35]NPY	>10,000	1	3	/	/	/	/	/	/	/	/	/	/	/	/	>4,900	>5	3	
[A36]NPY	1,378 (5.86 ± 0.06)	1	6	/	/	/	/	/	/	/	/	/	nd	nd	3	/	/	/	/
NPY-tyramide	68 (7.17 ± 0.11)	1	9	nd	nd	3	/	/	/	/	/	/	/	/	/	/	/	/	/

b. IP accumulation assays of WT Y ₁ R for NPY/NPY analogues							
	NPY	Ac-NPY	[A1]NPY	[A2]NPY	[A1,A2]NPY	NPY(3-36)	NPY(13-36)
EC ₅₀ (nM) (pEC ₅₀ ± SEM)	1.5 (8.83 ± 0.02)	0.5; 3.0	6.5; 2.4	7.3 (8.14 ± 0.11)	8.0 (8.10 ± 0.06)	83 (7.08 ± 0.09)	477; 744
X-fold over NPY	1	1; 2	4; 2	5	5	55	318; 496
n	51	2	2	4	3	3	2

c. NPY-induced IP accumulation assays of WT and mutant Y ₁ Rs										
	WT	F184 ^{ECL2} A	F184 ^{ECL2} N	V187 ^{ECL2} N	L189 ^{ECL2} N	Y192 ^{ECL2} S	V197 ^{ECL2} A	V197 ^{ECL2} N	F199 ^{ECL2} N	F202 ^{ECL2} N
EC ₅₀ (nM) (pEC ₅₀ ± SEM)	1.5 (8.83 ± 0.02)	18.7 (7.73 ± 0.08)	23 (7.64 ± 0.10)	1.9 (8.72 ± 0.08)	1.9 (8.73 ± 0.16)	3.8 (8.42 ± 0.11)	1.9 (8.71 ± 0.13)	188 (6.73 ± 0.11)	3.4 (8.47 ± 0.11)	1.2 (8.93 ± 0.15)
X-fold over WT	1	13	15	1	1	2.5	1	125	2	1
n	51	7	14	3	3	3	5	7	3	3

nd, not determined up to 10⁻⁴ M agonist concentration; /, not tested.

*Peptides were synthesized as described in the 'Peptide synthesis' section of the Methods.

†EC₅₀ values were determined using GraphPad Prism 5.0. All curves were normalized to the top and bottom values of the Y₁R-NPY curve. Nonlinear regression (curve fit) was performed for normalized response in all assays. All data are shown as mean values from at least three independent experiments or results of two individual experiments each performed in technical duplicate.

‡The EC₅₀ shifts were determined by EC₅₀(mutant)/EC₅₀(wild type). The Hill slope was set to one. For the wild-type receptor x-fold (fold change) is set to one. A lower EC₅₀ shift of the NPY analogue/mutant compared to NPY/mutant was interpreted as no further loss of function and a direct interaction between both positions.

§Sample size; the number of independent experiments performed in technical duplicate.

||Previously published data²⁷.

Extended Data Table 5 | Mass spectromeric signals and calculated mass of photo-crosslinked Y₁R with [Bpa¹, K⁴[(Ahx)₂-biotin]]NPY

MALDI-TOF MS (m/z)*	Number in Y ₁ R	Position [Bpa ¹ ,K ⁴ [(Ahx) ₂ -biotin]]NPY	M _{calc.} (Da)†	[M _{calc.} + H] ⁺ (Da)	[M _{calc.} + Na] ⁺ (Da)	[M _{calc.} + K] ⁺ (Da)
1824.2			not identified			
1867.3			not identified			
1892.6	11 - 32	1 - 6	3760.7	3761.8	3783.7	3799.7
1988.2	-	1-11 + 5-6	1986.9	1987.9	2009.9	2025.9
2001.1	-	1-10 + 5-7	2000.0	2001.0	2022.9	2038.9
2059.2	-	1-10 + 8-11	2057.9	2058.9	2080.9	2096.9
	-	1-11 + 8-10	2057.9	2058.9	2080.9	2096.9
2073.2			not identified			
	-	1-10 + 8-11	2057.9	2058.9	2080.9	2096.9
2081.3	-	1-11 + 8-10	2057.9	2058.9	2080.9	2096.9
2121.3			not identified			
2162.2	191 - 194	1 - 10	2139.0	2140.0	2162.0	2178.0
2311.4			not identified			
2317.4			not identified			
2381.4	191 - 195	1 - 11	2380.1	2381.1	2403.1	2419.1
2381.8	195 - 205	1 - 4	2381.1	2382.1	2404.1	2420.1
	32 - 32	1 - 16	2374.0	2375.0	2397.0	2413.0
2397.3	194 - 194	1 - 16	2374.0	2375.0	2397.0	2413.0
	21 - 21	1 - 16	2387.1	2388.1	2410.1	2426.1
2410.3	195 - 195	1 - 16	2387.1	2388.1	2410.1	2426.1
	194 - 195	1 - 15	2387.1	2388.1	2410.1	2426.1
2413.3	32 - 32	1 - 16	2374.0	2375.0	2397.0	2413.0
	194 - 194	1 - 16	2374.0	2375.0	2397.0	2413.0
2450.4	-	1-15 + 8-10	2427.1	2428.1	2450.1	2466.1
2514.5			not identified			
2553.5	194 - 200	1 - 10	2530.1	2531.1	2553.1	2569.1
2589.6			not identified			
2775.7			not identified			
2807.7			not identified			
3031.7	22 - 29	1 - 15	3030.4	3031.4	3053.4	3069.4
3377.7	191 - 200	1 - 15	3376.5	3377.5	3399.5	3415.5
3784.1	11 - 32	1 - 6	3760.7	3761.8	3783.7	3799.7
3966.3	-	1-7 + 17-36	3943.1	3944.1	3966.1	3982.1
4524.9			not identified			

*Determined signals by MALDI-TOF mass spectrometry.

†Selected calculated masses in Dalton of possible photo-crosslinked fragments of Y₁R with [Bpa¹, K⁴[(Ahx)₂-biotin]]NPY or [Bpa¹,K⁴[(Ahx)₂-biotin]]NPY with itself. The fragments are selected based on the correlation with the detected signals. For clarity, further calculated masses of possible photo-crosslinked fragments are not shown.

Life Sciences Reporting Summary

Nature Research wishes to improve the reproducibility of the work that we publish. This form is intended for publication with all accepted life science papers and provides structure for consistency and transparency in reporting. Every life science submission will use this form; some list items might not apply to an individual manuscript, but all fields must be completed for clarity.

For further information on the points included in this form, see [Reporting Life Sciences Research](#). For further information on Nature Research policies, including our [data availability policy](#), see [Authors & Referees](#) and the [Editorial Policy Checklist](#).

Please do not complete any field with "not applicable" or n/a. Refer to the help text for what text to use if an item is not relevant to your study. [For final submission](#): please carefully check your responses for accuracy; you will not be able to make changes later.

▶ Experimental design

1. Sample size

Describe how sample size was determined.

Due to radiation damage, X-ray diffraction data collection of the protein crystals was limited to 5-10 degree per crystal. To collect a complete data set for structure determination, diffraction data from multiple crystals were integrated and scaled using XDS. By calculating completeness of the data set, diffraction data from 47 Y1R-UR-MK299 crystals and 33 Y1R-BMS-193885 crystals were used to ensure the completeness was close to 100%. For the ligand binding, IP accumulation assays and NMR measurements, 2-5 independent experiments were performed in technical duplicate/triplicate to ensure each data point was repeatable.

2. Data exclusions

Describe any data exclusions.

No data were excluded from the analyses.

3. Replication

Describe the measures taken to verify the reproducibility of the experimental findings.

All attempts at replication were successful.

4. Randomization

Describe how samples/organisms/participants were allocated into experimental groups.

Randomization is not relevant to this study, as protein and crystal samples are not required to be allocated into experimental groups in protein structural studies, and no animals or human research participants are involved in this study.

5. Blinding

Describe whether the investigators were blinded to group allocation during data collection and/or analysis.

Blinding is not relevant to this study, as protein and crystal samples are not required to be allocated into experimental groups in protein structural studies, and no animals or human research participants are involved in this study.

Note: all in vivo studies must report how sample size was determined and whether blinding and randomization were used.

6. Statistical parameters

For all figures and tables that use statistical methods, confirm that the following items are present in relevant figure legends (or in the Methods section if additional space is needed).

n/a Confirmed

- The exact sample size (n) for each experimental group/condition, given as a discrete number and unit of measurement (animals, litters, cultures, etc.)
- A description of how samples were collected, noting whether measurements were taken from distinct samples or whether the same sample was measured repeatedly
- A statement indicating how many times each experiment was replicated
- The statistical test(s) used and whether they are one- or two-sided
Only common tests should be described solely by name; describe more complex techniques in the Methods section.
- A description of any assumptions or corrections, such as an adjustment for multiple comparisons
- Test values indicating whether an effect is present
Provide confidence intervals or give results of significance tests (e.g. P values) as exact values whenever appropriate and with effect sizes noted.
- A clear description of statistics including central tendency (e.g. median, mean) and variation (e.g. standard deviation, interquartile range)
- Clearly defined error bars in all relevant figure captions (with explicit mention of central tendency and variation)

See the web collection on [statistics for biologists](#) for further resources and guidance.

► Software

Policy information about [availability of computer code](#)

7. Software

Describe the software used to analyze the data in this study.

Phaser: version 2.5.6 (CCP4Interface 6.5.000)
REFMAC5: version 5.8.0103
BUSTER: version 2.10.3
COOT: version 0.7.2
SigmaPlot 11.0: Systat Software Inc., Chicago, IL;
GraphPad Prism Software 5.0: GraphPad Software, San Diego, CA

For manuscripts utilizing custom algorithms or software that are central to the paper but not yet described in the published literature, software must be made available to editors and reviewers upon request. We strongly encourage code deposition in a community repository (e.g. GitHub). [Nature Methods guidance for providing algorithms and software for publication](#) provides further information on this topic.

► Materials and reagents

Policy information about [availability of materials](#)

8. Materials availability

Indicate whether there are restrictions on availability of unique materials or if these materials are only available for distribution by a third party.

No unique materials were used.

9. Antibodies

Describe the antibodies used and how they were validated for use in the system under study (i.e. assay and species).

ANTI-FLAG M1 from mouse: Sigma, order no. F3040, lot SLBK1592V, diluted 1:500.
anti-mouse IgG HRP-conjugated antibody from goat: Sigma, order no. A0168, lot 080M4839, diluted 1:80,000.

10. Eukaryotic cell lines

a. State the source of each eukaryotic cell line used.

COS-7 cells were obtained from American Type Culture Collection (ATCC). Sf9 cells were obtained from Invitrogen.

b. Describe the method of cell line authentication used.

The COS-7 cell line was authenticated using a PCR based multiplex assay based on the use of short tandem repeats (STR) (Authentication of Human Cell Lines: Standardization of STR Profiling, ANSI/ATCC ASN-0002-2011). The Sf9 cell line was authenticated through morphology check by microscope and growth curve analysis.

c. Report whether the cell lines were tested for mycoplasma contamination.

The cell lines were negative for mycoplasma contamination.

d. If any of the cell lines used are listed in the database of commonly misidentified cell lines maintained by [ICLAC](#), provide a scientific rationale for their use.

No commonly misidentified cell lines were used.

► Animals and human research participants

Policy information about [studies involving animals](#); when reporting animal research, follow the [ARRIVE guidelines](#)

11. Description of research animals

Provide all relevant details on animals and/or animal-derived materials used in the study.

No animals were used.

Policy information about [studies involving human research participants](#)

12. Description of human research participants

Describe the covariate-relevant population characteristics of the human research participants.

The study did not involve human research participants.